Analysis of Pluto's Light Curve to Detect Volatile Transport

by

Megan Mansfield

Submitted to the Department of Earth, Atmospheric, and Planetary Sciences
in partial fulfillment of the requirements for the degree of

Bachelor of Science in Earth, Atmospheric, and Planetary Sciences

at the

MASSACHUSETTS INSTITUTE OF TECHNOLOGY

June 2016

Author ..... Signature redacted .....
Department of Earth, Atmospheric, and Planetary Sciences
May 6, 2016

Certified by ..... Signature redacted .....
Amanda Bosh
Senior Lecturer
Thesis Supervisor

Accepted by . Signature redacted .....
Tanja Bosak
Chairman, Department Committee on Undergraduate Theses

Analysis of Pluto's Light Curve to Detect Volatile Transport

by

Megan Mansfield

Submitted to the Department of Earth, Atmospheric, and Planetary Sciences
on May 6, 2016, in partial fulfillment of the
requirements for the degree of
Bachelor of Science in Earth, Atmospheric, and Planetary Sciences

Abstract

Changes in the volatile distribution on Pluto's surface and in its atmosphere are expected to occur over its orbital path due to varying surface insolation[14]. To investigate these changes, a model was created to synthesize light curves of Pluto, given the viewing geometry and surface albedo distribution. Using an initial surface albedo distribution based on images taken by New Horizons, changes in the light curve mean magnitudes and amplitudes over time were compared to the smallest magnitude changes detectable by a variety of telescopes. The model predicts that yearly observations on a large ground-based telescope, such as the 6.5-meter Magellan telescopes, could observe magnitude changes due to both changes in viewing geometry and surface albedo changes. The model can be compared to future observations to estimate how much surface albedo change is necessary to produce the observed light curves, and can therefore be used to link observational data to physical changes on Pluto's surface and the methods of volatile transport responsible for those changes.

Thesis Supervisor: Amanda Bosh
Title: Senior Lecturer

Acknowledgments

Megan Mansfield gratefully acknowledges Amanda Bosh, Molly Kosiarek, Mike Person, and Tim Brothers for their assistance in collecting, analyzing, and interpreting data.

Contents

List of Figures

List of Tables

Chapter 1

Introduction

Pluto has an eccentric orbit such that its distance from the sun varies between 30 and 50 astronomical units. In addition, its obliquity of 120° and orbital period of 248 years mean that over the course of its orbit the amount of sunlight its different hemispheres receive varies by a large amount. This variation is expected to cause the migration of volatiles such as nitrogen, carbon monoxide, and methane across Pluto's surface[14]. This migration would be detectable as changes in Pluto's light curve, because the icy frosts moving across the surface would have a higher albedo than the material beneath them, and new ice condensing out onto the surface would be brighter than the old material it covers up[5].

Modeling the amount of sunlight received at Pluto is important to understanding its surface albedo distribution, because changes in the insolation across different latitudes could cause volatile transport. Earle and Binzel (2015) modeled the insolation of Pluto at different points in its orbit and calculated the average insolation at different latitudes over varying timescales[6]. In the current epoch, they found that the maximum average insolation was at Pluto's North Pole, while the minimum insolation was at the South Pole[6]. This difference is due to the fact that, over the past 30 years, Pluto has been rotating so that its North Pole points more and more directly toward the Sun. Currently, the North Pole is receiving constant sunlight, while the South Pole is always facing away from the Sun. Over longer timescales that lasted one or more orbits, the poles received more insolation than the equator.

They also calculated the Maximum Diurnal Insolation (MDI), which is the maximum insolation at any latitude on a given day in Pluto's orbit. They found that at Pluto's current position, with its North Pole pointing toward the Sun, the MDI is highest at the North Pole[6]. Additionally, the MDI at the North Pole is currently higher than the MDI at any point on the surface when the equator was facing the Sun[6]. They observed a possible correlation between the MDI and the atmospheric pressure, which could indicate that the differences in insolation at different orientations are a driving force behind the sublimation and transportation of volatiles[6].

In addition to understanding how insolation could drive volatile transport, modeling can be used to predict how surface volatile distributions would change depending on their composition and properties. Spectral observations of Pluto suggest that the main volatile present on its surface is nitrogen, but it also contains significant amounts of methane and carbon monoxide[1]. Images from the New Horizons flyby in July 2015 suggest that these volatiles are present in gaseous and solid states over a solid water ice "bedrock" layer[11]. Early models of volatile transport on Pluto focused on the sublimation and condensation of nitrogen[9]. Hansen and Paige (1996) adapted a model of nitrogen transport on Triton to fit conditions on Pluto[9]. Their model's parameters included the albedo and emissivity of frost on Pluto, the albedo and thermal inertia of the surface under the frost, and the total amount of nitrogen on the ground and in the atmosphere. They found that observations of Pluto were best matched by a bright frost on top of a dark substrate[9]. Additionally, they predicted that a surface with a high thermal inertia would produce zonal bands of frost, while a surface with a moderate thermal inertia would produce bands of frost closer to the poles and polar spots without any frost[9].

A second model of nitrogen transport was described in Young (2013). In a manner similar to the Hansen and Paige (1996) model, this model took into account the bolometric hemispheric albedo and emissivity of both the nitrogen ice and the underlying substrate, as well as Pluto's thermal inertia and the total amount of nitrogen. After testing a variety of values for these parameters, they discarded any sets of parameters that did not match the properties of Pluto determined from observations of stel-

lar occultations[14]. They found three categories of models, based on where volatiles were located. The first set of models were classified as "permanent northern volatiles," because they had permanent deposits of volatiles on the northern hemisphere. The second class were called "exchange with pressure plateau," and were characterized by polar caps of volatiles that remained for a long time after Pluto's perihelion equinox. In this case, volatiles were slowly exchanged between the two hemispheres until all the volatiles had been exchanged. The third group of models were called "exchange with early collapse," and showed situations in which northern volatiles disappeared rapidly after the time of Pluto's perihelion. In this set of models, like in the second set, volatiles were completely exchanged between Pluto's two hemispheres. Unlike Hansen and Paige (1996), who predicted the possibility of bright zonal bands of frost and darker poles, Young (2013) predicted that Pluto should generally have brighter poles and darker equatorial areas[9, 14]. The Young (2013) pattern of brighter poles and darker equatorial regions is closer to what was observed by New Horizons, which saw a bright North Pole and a generally dark equatorial band, except for the brighter Tombaugh Regio[11].

Photometric observations of Pluto can be used to confirm or contradict the predictions made by these models. Buratti et al. (2003) created a light curve of Pluto and compared it to historical light curves[5]. They found that the amplitude of Pluto's light curve had increased over time. However, using a model of Pluto based on the surface map created by Stern et al. (1997) from Hubble observations of Pluto, they found that this increase could be explained by changes in viewing geometry alone, and that at this point there was no evidence of volatile transport on Pluto[12, 5]. They also found that Pluto's color had stayed constant over past observations[5]. Buie et al. (2010a) made a light curve of Pluto using similar techniques and found a smaller light curve amplitude[2]. They determined that this difference was also due to viewing geometry, not volatile transport, as Pluto's pole was pointing closer to the Earth than it had been for past measurements of its light curve[2]. Because the pole was pointing closer to the Earth, there was less variation in what part of Pluto's surface was visible from Earth over one period, and so a smaller amplitude was ex-

pected due to geometry alone[2]. They also detected a reddening of Pluto's light curve, and suggested that Pluto had been reddening between 2000-2003[2]. In addition to determining properties of Pluto, they were able to study Charon separately because their observations using the Hubble Space Telescope were able to spatially resolve Pluto and Charon. They found that Charon's brightness and color had been the same since previous measurements completed in 1993[2, 3]. This is significant because, if Charon's brightness and color are constant, any changes in a light curve can be assumed to be due to changes on Pluto's surface, even if the observations can not spatially resolve Pluto and Charon.

Buratti et al. (2015) made a light curve of Pluto and compared its shape and amplitude to past light curves to conclude that volatile transport was occuring on Pluto. Additionally, using the same model as in Buratti et al. (2003), they found that the light curve amplitudes after 2002 can not be explained as an effect of viewing geometry changes alone[5, 4]. Therefore, they suggested that volatile transport has been happening on Pluto's surface since 2002[4]. They also observed reddening in Pluto's albedo, and suggested that it could be due to a red substrate being uncovered as the volatiles above it sublimate[4].

Recently, the New Horizons mission allowed more exact information on Pluto's surface albedo to be measured. Pluto's equatorial area contains both very dark and very bright material. The bright Tombaugh Regio has a radiance factor around 0.85, and is possibly a reservoir of icy volatiles[8, 11]. The darker Cthulhu Regio has a radiance factor of 0.15[8]. These exact measurements can inform models to match past measurements with surface albedo characteristics.

The intent of this project was to model the changes in Pluto's light curve due to changes in both its viewing geometry and its surface albedo. A model was created that, given a surface albedo map and a sub-observer latitude, predicts a light curve. Section 2 describes the model and uses it to predict what Pluto's light curve would look like when observed on the 16-inch telescope at Wallace Observatory. To confirm the model's predictions, Pluto was observed during September-November 2015 using the 16-inch telescope at Wallace Observatory (Section 3). Section 4 compares the

model to the observations to determine what changes on Pluto's surface would be detectable from Wallace Observatory and from other telescopes. Finally, Section 5 discusses how this model can be used in the future to inform telescope choice when observing Pluto and to interpret resulting light curves.

Chapter 2

Lightcurve Model

2.1 Modeling Pluto's Light Curve

A simple model of Pluto's rotational light curve was generated using an albedo map of the surface. A rough map of the reflectance of Pluto's surface was generated using measurements taken by New Horizons as reported by Grundy et al. (2016)[8]. The surface was divided into five main regions of different albedos, which are outlined in Table 2.1. All other areas on the surface of Pluto were assigned an albedo of $\alpha = 0.5$, which was the average albedo of the planet as a whole as reported by New Horizons[8]. The entire albedo map had a resolution of 1° in both latitude and longitude. Fig. 2-1 shows the map generated from this rough approximation.

In addition to this simplified albedo map, the model also used the current sub-observer latitude, B, to calculate which latitudes and longitudes are visible from Earth at any given time. Values for B were found for each year of interest using the JPL HORIZONS web interface [7].

Using these two inputs, the model steps through each degree of longitude and, for each degree, calculates the mean albedo of all visible points. The albedos of each point are weighted by $\cos(\lambda)$ to account for projection effects and by $(\cos(\lambda - \lambda_B))(\cos(\phi - \phi_B))$ to account for the fact that points closer to the subobserver point will reflect more of their light directly toward the Earth[5]. In these weights, λ and ϕ are the latitude and longitude of the point on Pluto's surface, and λ_B and ϕ_B are the sub-

Table 2.1: Primary albedo regions in the Pluto model

Region Name	Albedo	Latitude Range	Longitude Range
Sputnik Planum	0.85	−20°- 40°	160°- 195°
Tombaugh Regio Edges	0.8	−30°- −20°	150°- 200°
		0°- 30°	195°- 240°
Cthulhu Regio	0.15	−20°- 0°	15°- 40°
		−20°- 10°	40°- 160°
		−30°- −20°	110°- 150°
Dark Equatorial Regions	0.3	−20°- 0°	195°- 230°
	0.4	−15°- 0°	255°- 300°
		−20°- 0°	310°- 325°
		−20°- 0°	345°- 355°
North Polar Cap	0.7	60°- 90°	1°- 360°

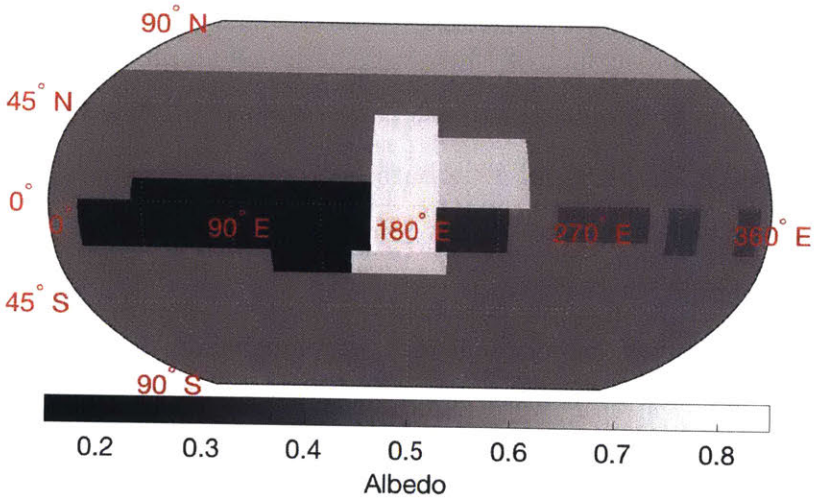

Figure 2-1: A simple albedo map of Pluto that was used as the input to the model described in Section 2.1. The map is based on images of Pluto taken by New Horizons during its July 2015 flyby [8].

observer latitude and longitude, respectively. This model assumes all measurements are made at zero phase angle, which is a valid assumption because the phase angle of Pluto never gets larger than $\approx 1.9°$.

The model output the mean albedo visible at each degree of sub-observer longitude, from which a synthetic light curve could be constructed. The mean albedo for each longitude point was converted into a magnitude for visible light using the equation

$$m_{pl} = m_{\odot} - 2.5 \log_{10}(\frac{\alpha d_{es}^2 r_{pl}^2}{4 d_{ps}^2 d_{ep}^2}), \tag{2.1}$$

where m_{pl} is the magnitude of Pluto, $m_{\odot} = -26.7$ is the magnitude of the Sun in the visible wavelengths, α is the mean albedo, $d_{es} = 1.496 * 10^{11}$ m is the J2000 Earth-Sun distance, $r_{pl} = 1.187 * 10^6$ is Pluto's radius, and d_{ps} and d_{ep} are the J2000 Pluto-Sun distance and the J2000 Pluto-Earth distance at the time of observation, respectively.

The synthetic light curves were compared to each other using two main metrics. The amplitude of each light curve was calculated by subtracting the brightest point from the darkest point in the light curve. The mean of each light curve was also calculated and used to find the net change in Pluto's mean magnitude between the time of observation and the time of the New Horizons flyby of Pluto in July 2015.

This model only considers the light curve due solely to light reflected from Pluto, and neglects the light reflected from Charon. However, Charon's surface is nearly featureless, and its light curve has not changed significantly in the past 15 years, so it is valid to assume that Charon's surface albedo has been and will remain nearly constant [11, 2]. The difference between the magnitude of the combined Pluto-Charon system and the magnitude of Pluto alone is a constant $\Delta m = 0.2$, but the addition of Charon will not change the measured light curve amplitude[3]. Furthermore, the addition of Charon would not affect the measurement of the change in mean magnitude over time. Therefore, for this model, Charon can be neglected.

2.2 Model Interpretation and Predictions

The model can be used in two primary ways to predict the observability of Pluto over time. First, it can be used to generate synthetic light curves for observations of Pluto in the past and future, assuming that Pluto's surface albedo is constant over time. This version of the model accounts only for changes in the light curve due to viewing geometry changes, and can be used to predict what the light curve would look like if Pluto's surface albedo is static.

Second, the model can explore how changes in surface albedo affect the resulting light curve. Changing the initial albedo map that the model uses as an input can produce light curves showing the effects of those albedo changes on the overall mean visible magnitude of Pluto and the light curve amplitude. The North Pole is currently pointing almost directly at the Sun and will continue to receive constant sunlight for many years, so the most likely change in Pluto's albedo distribution as visible from the Earth over the next few years is a darkening of the North Pole area. This darkening would be due to ices on the North Pole sublimating and revealing the darker substrate underneath. In this scenario, some ices may be condensing near Pluto's South Pole and raising the albedo of that area, but this effect is not observed from Earth because only the North Pole area is visible from Earth.

It is possible that other albedo changes could happen on Pluto's surface that would affect the area currently observable from the Earth. For example, changes in the albedo distribution in the equatorial regions could affect the amplitude of the light curve. However, this paper mainly focuses on an overall darkening of the polar region, for two main reasons. First, as mentioned above, darkening of the North Pole region is expected due to the higher insolation in that area compared to the equatorial and southern regions [6]. Second, because Pluto's pole is pointing almost directly at the Earth, there are only small variations in the part of the planet that is visible over one period. Therefore, over the next few years, changes that affect Pluto's overall mean magnitude will be easier to detect than changes that would affect the light curve amplitude, and changes in the polar region will be easier to detect than

changes closer to the equator.

Before applying the model, two tests were conducted to ensure the model's accuracy. First, the model's output for a Pluto in which the surface albedo distribution does not change over time was compared to a similar static-albedo model generated by Buratti et al. (2003) [5]. Fig. 2-2 shows a comparison between the light curve amplitudes predicted by our model and the model generated in Buratti et al. (2003). The two models produce similar amplitudes over time, suggesting that our model reproduces the static-albedo results of Buratti et al. (2003) to a high degree of accuracy. Both models ignore the contribution to the light curve from Charon, so this did not cause the difference between the calculated amplitudes[5]. The slight difference between the amplitudes predicted by the two models could be due to the fact that they rely on different sets of observations to produce the maps of Pluto's surface albedo. Buratti et al. (2003) based their model on surface albedo maps generated by Stern et al. (1997) using HST observations[5, 12]. Comparing the Stern et al. (1997) maps to the Grundy et al. (2016) map used to create this model shows some differences in the recorded surface features[12, 8]. In particular, Stern et al. (1997) saw bright spots in the Southern hemisphere, at latitudes below where New Horizons was able to measure the albedo[12, 8]. Stern et al. (1997) also saw darker regions in the Northern hemisphere where Grundy et al. (2016) measured a brighter North Pole region[12, 8]. These differences between the two maps would translate to differences in the light curve amplitudes of the models. However, the close match between the two models indicates that the largest features that have the most impact on the observed light curve were accurately described in both cases. The model created in this paper could also be slightly off from the Buratti et al. (2003) model because of the low resolution at which the main albedo features were represented in the model. However, tests of the model indicate that the large surface features such as Tombaugh Regio and Cthulhu Regio are most important to reproducing historical light curves, and more minor albedo features do not affect the light curve significantly.

Second, observations were completed at Wallace Observatory to compare the predicted light curve to an observed light curve. Fig. 2-3 shows the light curve ampli-

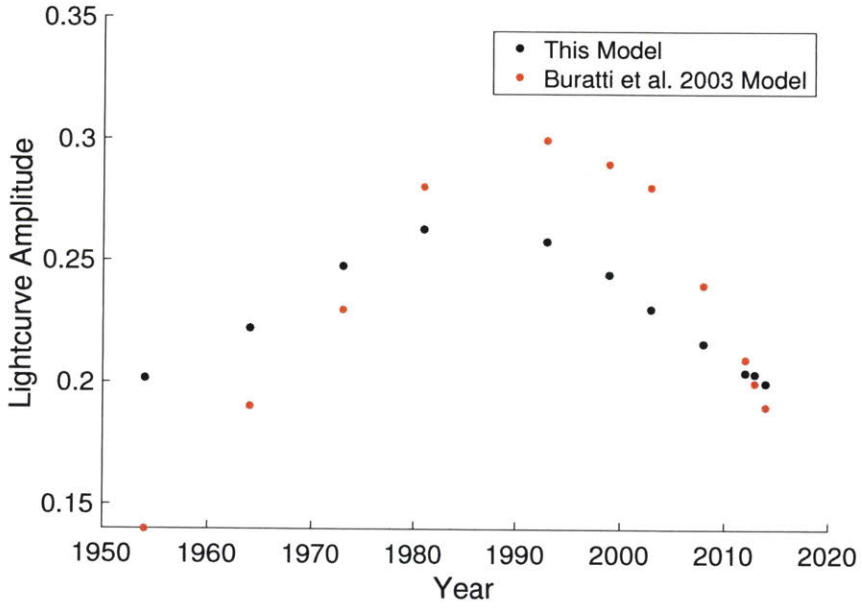

Figure 2-2: A comparison of light curve amplituded for a model in which Pluto's albedo is not changing over time. Black points represent amplitudes for light curves generated by the model described in Section 2.1. Red points represent amplitudes for the model described in Buratti et al. (2003) [5]. The two models produce similar amplitudes, suggesting that our model predicts light curve amplitudes and mean magnitudes with an accuracy similar to that of Buratti et al. (2003).

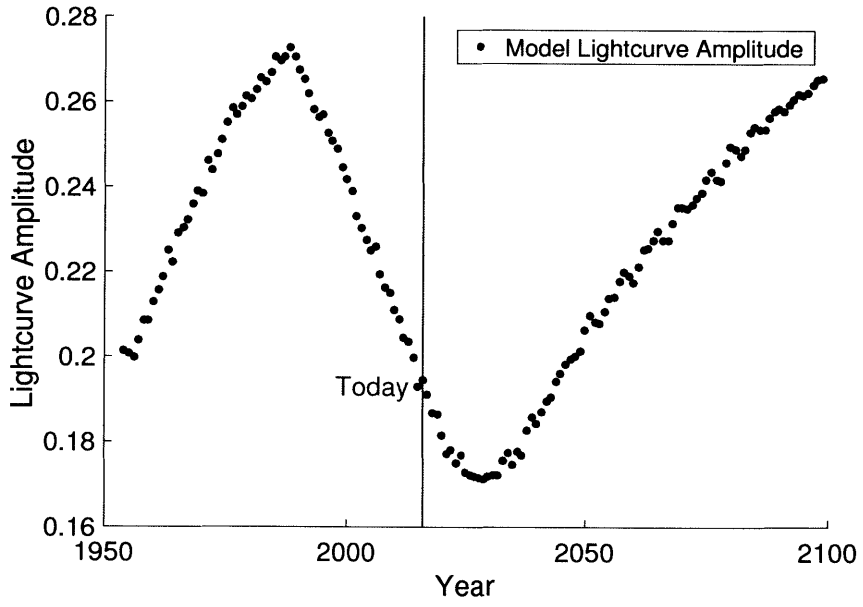

Figure 2-3: Light curve amplitude over time generated by a model in which Pluto's albedo distribution is constant. From this static-albedo model, Pluto's light curve should have an amplitude of about $\Delta m = 0.1990$ in October 2015.

tude predicted by a model with a constant albedo distribution for each year between 1954 (the year of the first observations included in Buratti et al. (2003)) and 2100. From the output of the static-albedo model, the light curve amplitude should be $\Delta m = 0.1990$ in October of 2015, which is when the observational data were collected at Wallace Observatory. While this predicted light curve amplitude is only based on the static-albedo model, it is unlikely that Pluto's global albedo distribution would change significantly between the New Horizons visit in July 2015 and the observations in October 2015 because Pluto's long orbital period of 248 years means that changes should happen over timescales longer than a few months. The observations at Wallace Observatory, the reduction and analysis of the observations, and a comparison of the observations to the model predictions are outlined in Section 3.

Chapter 3

Observing Pluto's Lightcurve

3.1 Observations

To test the model's ability to predict observability, Pluto was observed using the 16-inch telescope and the 14-inch telescope on Pier 3 at Wallace Observatory ($\phi = 42°36.6'$, $\lambda = -71°29.1'$) in Westford, Massachusetts. Instrumental specifications for the telescope are shown in Table 3.1. Pluto was observed on fifteen nights between September and November 2015, and these observations are summarized in Table 3.2. Pluto was observed in the Johnson R filter because this filter has been used for past observations, and so comparisons can be made to historical light curves[4, 5]. The exposure time on all images was approximately 30-40 seconds, because this exposure time allowed a good signal-to-noise ratio for Pluto without having excessively high background count levels. On each observing night, between 30 minutes and 3 hours of data were collected.

Table 3.1: Instrument specifications for the telescopes at Wallace Observatory used to observe Pluto.

Pier	3	16
Diameter (in.)	14	16
Viewing Window Size	20.65x20.65 arcmin.	19.07x19.07 arcmin.
Plate Scale	1.21 arcsec./px	1.11 arcsec./px

Table 3.2: Details of observing conditions for each night of data collection.

Date	Conditions	Pier	Pluto RA, Dec (J2000)	Filter	Focuser	Number of Images	Exposure Time (s)
2015/09/19	Started clear, got cloudy at the end of the night	3	18:54:43.9, -21:00:49.0	R	2657	76 science, 10 bias, 10 dark	60
		16			4651	92 science, 10 bias, 10 dark	30
2015/09/20	Very clear, quarter moon	16	18:54:43.2, -21:00:59.1	R	4850	140 science, 10 bias, 10 dark, 10 flat	40 (1 for flats)
2015/09/24	Very clear, nearly full moon	16	18:54:41.8, -21:01:47.0	R	4450	177 science, 10 bias, 10 dark	40
2015/09/26	Partly cloudy, nearly full moon	16	18:54:42.2, -21:02:05.0	R	6000	8 science, 10 bias, 10 dark	40
2015/09/27	Very clear, full moon, lunar eclipse	16	18:54:42.2, -21:02:05.1	R	5000	147 science, 10 bias, 10 dark	30
2015/10/10	Very clear	16	18:54:59.1, -21:03:51.5	R	5500	10 science, 10 bias, 10 dark	40
2015/10/11	Very clear, a few wispy clouds later in the evening	16	18:55:01.3, -21:03:57.7	R	5100	57 science, 10 bias, 10 dark	30
2015/10/12	Very clear	16	18:55:03.6, -21:04:03.7	R	4851	79 science, 10 bias, 10 dark	30
2015/10/16	Clear	16	18:55:14.2, -21:04:26.0	R	5400	11 science, 10 bias, 10 dark	30

2015/10/18	Patchy clouds	16	18:55:20.2, -21:04:36.0	R	6251	25 science, 10 bias, 10 dark	30
2015/10/23	Clear, 3/4 moon	16	18:55:37.5, -21:04:57.5	R	5850	20 science, 10 bias, 10 dark	40
2015/10/26	Clear, full moon, a few wisps of cloud late in the evening	16	18:55:49.0, -21:05:08.0	R	5700	16 science, 10 bias, 10 dark, 12 flat	40 (1 for flats)
2015/10/30	Clear	16	18:56:06.6, -21:05:19.5	R	5551	18 science, 10 bias, 10 dark	30
2015/11/03	Very clear	16	18:56:26.1, -21:05:27.8	R	5000	24 science, 10 bias, 10 dark	30
2015/11/04	Clear	16	18:56:30.7, -21:05:29.3	R	4482	17 science, 10 bias, 10 dark	30

During the months of observation, Pluto's J2000 right ascension was between $\alpha = 18:54:43.9$ and $\alpha = 18:56:30.7$, and its J2000 declination was between $\delta = -21:00:49.0$ and $\delta = -21:05:29.3$. Fig. 3-1 is a finder chart with the positions of Pluto on each night of observing marked by red circles. Its apparent magnitude was approximately $m = 14.2$, and the Pluto-Earth distance was approximately $\Delta = 33$ AU.

The two main complications to data collection during this period were Pluto's position in the plane of the Milky Way and its location near the horizon. Because Pluto was in the plane of the Milky Way, it was in a crowded starfield, so apertures had to be carefully designated to avoid measuring any background stars. In addition, Pluto was near the horizon and setting early throughout the data collection time period. The larger airmass near the horizon lessened the quality of the images obtained. The position near the horizon also limited the duration of each night of observing.

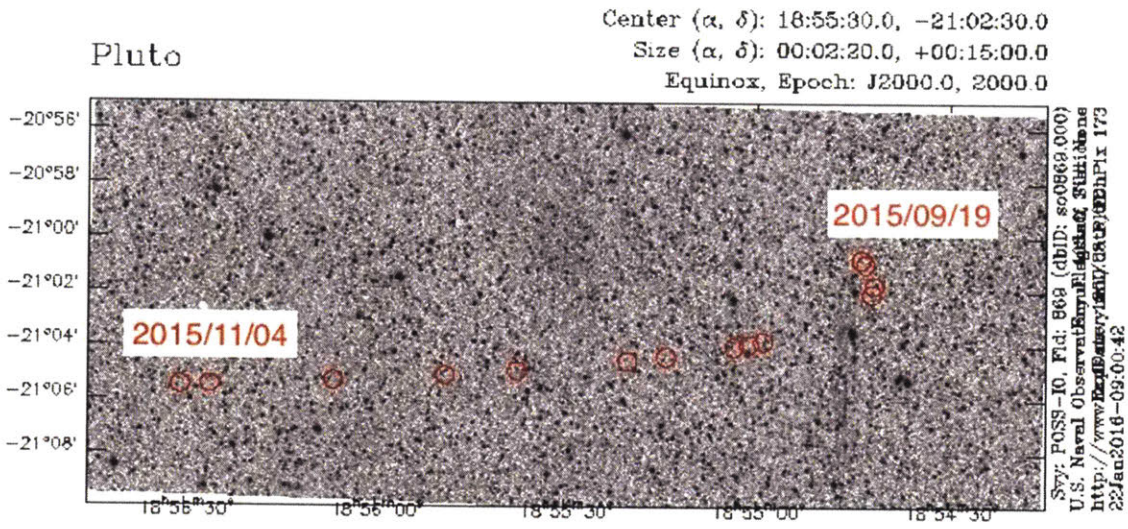

Figure 3-1: Finder chart used to identify the position of Pluto. The red circles indicate the position of Pluto on each night of observing, with the rightmost and leftmost circles marked with the date on which Pluto was in that position.

Data collection ended in the first week of November because, at this point, Pluto was setting around 11:30 PM UT, less than half an hour after twilight at Wallace Observatory.

3.2 Data Reduction and Analysis

3.2.1 Data Reduction and Standard Star Selection

Data reduction was completed using the software package AstroImageJ. Bias and noise were removed using biases, darks, and flats taken throughout observing. The signals from Pluto and 6-20 on-chip comparison stars were measured in each image. In October 2015, Pluto moved an average of 0.0090 arcseconds during a 40-second exposure. This is equivalent to 0.0082 pixels across the CCD on the 16-inch telescope or 0.0074 pixels across the CCD on the 14-inch telescope, so its motion over the course of an individual image was neglected.

Aperture sizes were selected to encompass the entirety of Pluto's signal. Fig. 3-2 shows an example of the graphs created using AstroImageJ that were used to

determine the aperture size on each night of observations. The aperture size was adjusted for each night of data to account for changes in seeing, and was between 5 and 10 pixels in radius. Background apertures were designated as circular annuli around the target apertures. The locations of background and target apertures were checked to ensure that none contained background stars.

On three nights - September 24, October 12, and November 3, 2015 - background stars were located close enough to Pluto that in some images Pluto's signal overlapped with that of the star. Therefore, on these three nights, larger apertures were designated that contained both Pluto and the background star. Images of the same fields were taken on days when Pluto was in a different location, and these images were used to measure the magnitudes of the background stars relative to APASS standard stars. Using these magnitudes, the background star signals were subtracted from the apertures containing Pluto and those background stars.

The on-chip comparison stars were selected from the APASS standard star catalog. All comparison stars with Sloan r' magnitudes between $m_r = 13$ and $m_r = 14$ were initially selected and their signals were compared to each other to check for variability. The comparison stars were also checked to ensure that none of them had anomalously large or small B-V colors, because the color correction applied later using Eq. 3.2 is slightly color-dependent. Fig. 3-3 shows an example of the plots created to determine which comparison stars to use. All non-variable stars with normal B-V colors in this magnitude range that were within 0.1° of the center of the image were used to calculate the magnitude of Pluto. Table A.1 in Appendix A contains information on the magnitudes and positions of the standard stars used on each night. The final magnitude of Pluto on each night was found by taking a weighted mean of the signals from Pluto relative to each of the standard stars, and then converting that weighted mean to a magnitude scale.

Pluto's moon, Charon, is too close to Pluto to be spatially resolved in images taken on the 16-inch telescope at Wallace Observatory. Therefore, the calculated Pluto magnitudes actually represent the combined magnitudes of the Pluto-Charon system. However, Charon is much fainter than Pluto, and so 84% of the visible light is

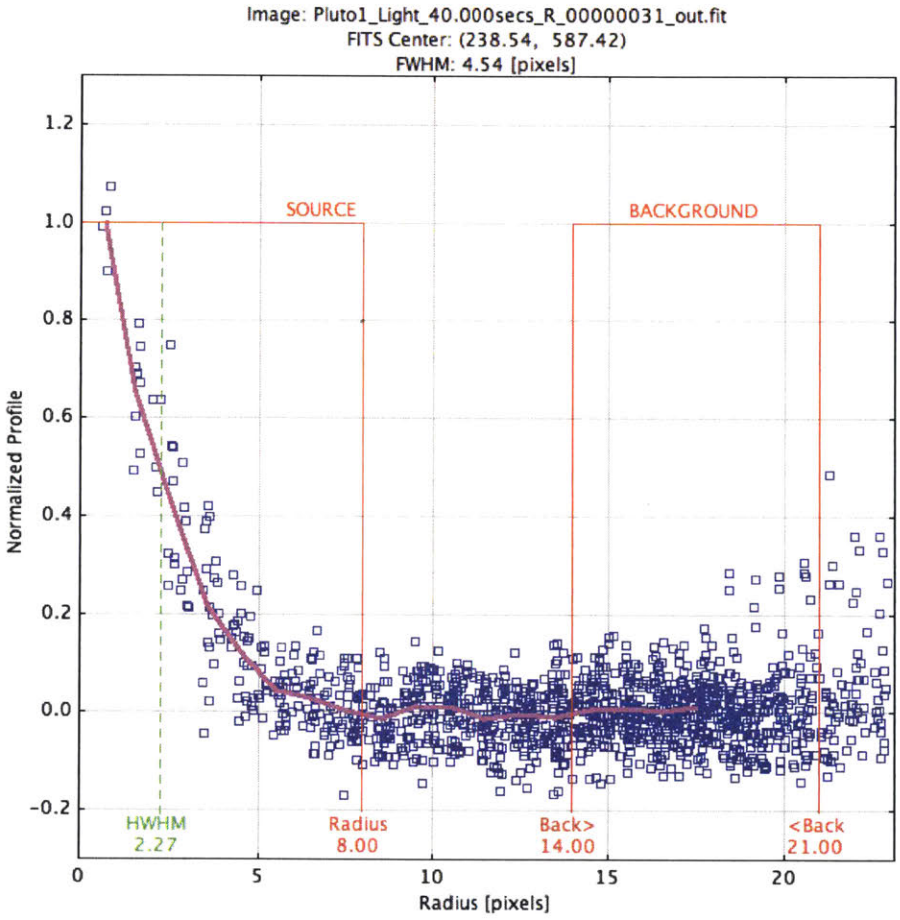

Figure 3-2: An example of the graphs used to determine the aperture size on each image of Pluto. This signal profile is a measurement of Pluto on an image taken on October 10, 2015. Blue data points indicate normalized pixel values as a function of the radius from the center target pixel. The green dotted line marks the location of the half width at half maximum (HWHM), while the red lines indicate the outer radius of the target aperture and the inner and outer radii of the background aperture. On each night, the aperture size was adjusted to contain all of Pluto's signal.

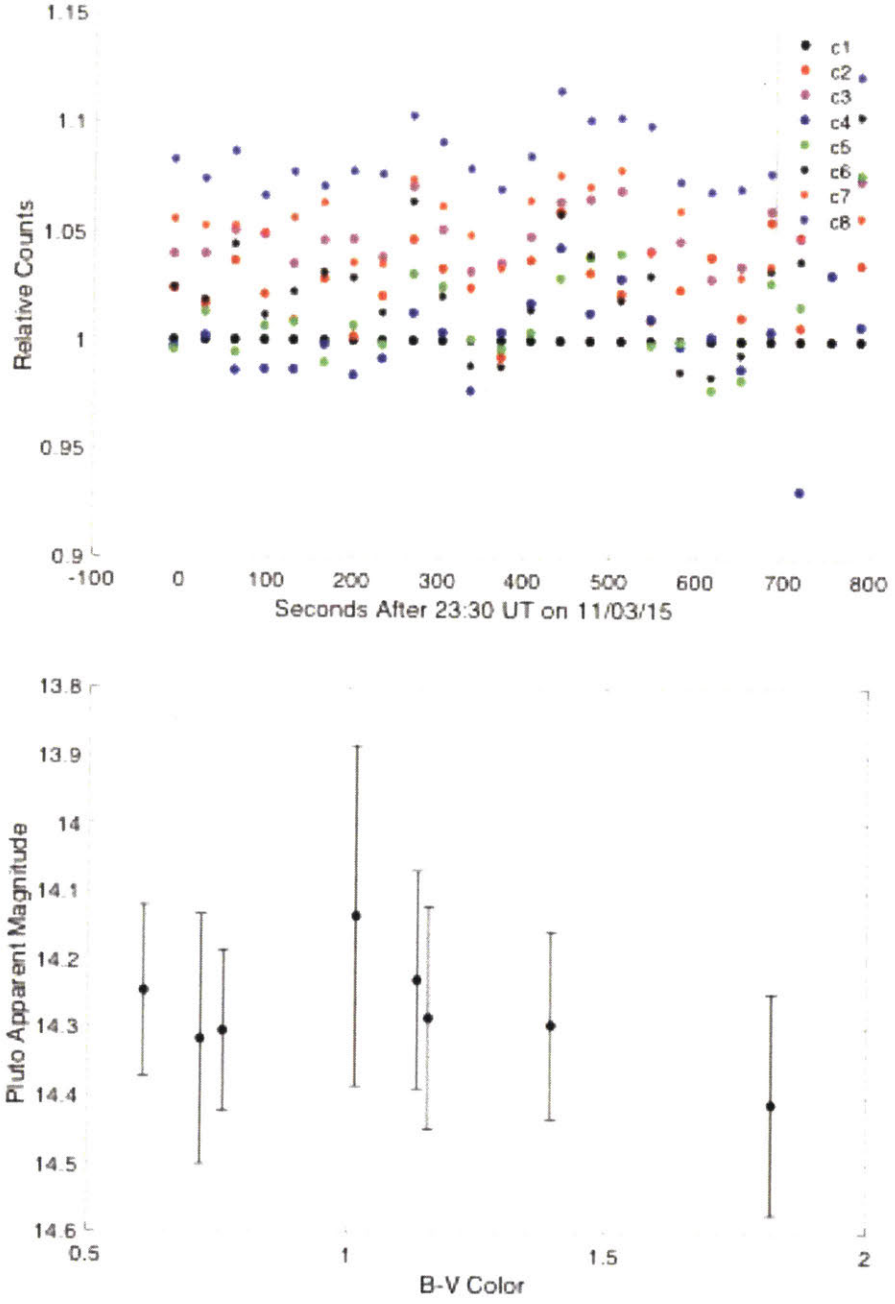

Figure 3-3: An example of the figures created to verify which APASS comparison stars could be used to calculate the magnitude of Pluto. These figures display data for the on-chip comparison stars from November 3, 2015. The top figure plots the signal from each comparison star divided by the signal from the first comparison star, while the bottom figure plots the B-V color of each comparison star against the magnitude of Pluto calculated from using that comparison star. From the top figure, none of the stars were variable. However, from the bottom figure, one comparison star had $B - V = 1.817$, which was large compared to the rest of the comparison stars. This star was discarded before the final calculation of Pluto's magnitude.

due to Pluto, and the difference between the magnitude of the combined Pluto-Charon system and the magnitude of Pluto alone is $\Delta m = 0.2$[3]. In addition, the difference in brightness between Charon's two hemispheres is only about 8% of its overall brightness, and its light curve has not changed significantly in the past 15 years[2]. The light curve amplitudes and mean opposition magnitudes calculated in Buratti et al. [2015] are based on the combined Pluto-Charon signal, so leaving Charon's signal in the data also allows direct comparison to these past measurements[4].

3.2.2 Light Curve Creation

After using AstroImageJ to measure the signals from each source of interest, the remaining data analysis was done using MATLAB. Each night of observation covered $0.33 - 1.3\%$ of Pluto's 6.4-day rotational period, so each night produced one data point on Pluto's rotational light curve. To create a light curve from the raw data, the data had to be corrected for differences in the Pluto-Earth distance at the time of observation and the Pluto-Sun distance at the time of observation. All data points were corrected to the mean opposition distance between Pluto and the Earth ($\Delta_0 =$ 38.5 AU) and the mean opposition distance between Pluto and the Sun ($r_0 = 39.5$ AU) using the equation

$$m_0 = m + 5\log_{10}(\Delta_0 r_0) - 5\log_{10}(\Delta r), \tag{3.1}$$

where Δ is the Pluto-Earth distance at the time of observation, r is the Pluto-Sun distance at the time of observation, m is the observed apparent magnitude, and m_0 is what the apparent magnitude would be at $\Delta_0 = 38.5$ AU and $r_0 = 39.5$ AU. These distances were chosen to match the distance corrections in Buratti et al. (2015) to make comparisons between the two data sets simpler[4].

In addition to these geometry corrections, a correction was applied to account for the fact that the APASS standard stars have known magnitudes in the B, V, g', r', and i' filters, but the images were taken in the R filter. This correction was applied

using the equation

$$g - r = (1.646 \pm 0.008)(V - R) - (0.139 \pm 0.004) \tag{3.2}$$

from Jordi et al. (2006), where g, r, V, and R are the apparent magnitudes of the star in the Sloan g', Sloan r', Johnson V, and Johnson R filters, respectively[10]. Fig. 3-4 shows the final light curve after applying these magnitude corrections. The light curve is phase-folded using the east subobserver latitude at the time of observation.

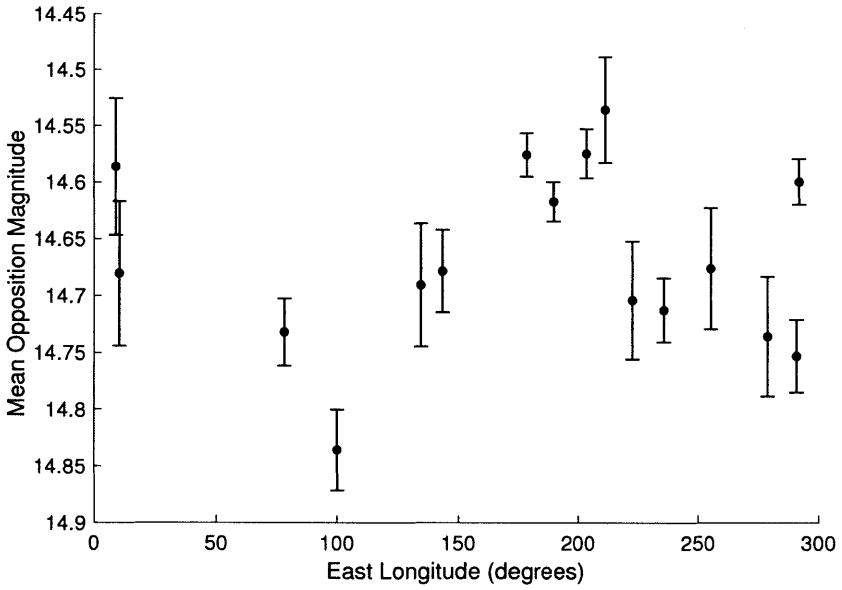

Figure 3-4: Pluto light curve, created from observations in September-November 2015. The figure plots the east subobserver longitude against the mean opposition magnitude of Pluto, which accounts for corrections due to differences in viewing geometry and telescope filter.

3.3 Observational Results

The final light curve was compared to the results of Buratti et al. (2015), as shown in Fig. 3-5. The red line in Fig. 3-5 is the fitted line to the R-filter light curve from Buratti et al. (2015), whose equation is given by

$$m(\theta,\alpha) = -0.0263\sin(\theta) + 0.0128\sin(2\theta) - 0.00180\sin(3\theta) \\ - 0.0155\cos(\theta) + 0.00950\cos(2\theta) + 0.00302\cos(3\theta) + \beta\alpha, \quad (3.3)$$

where θ is the east subobserver longitude, α is the phase angle, and $\beta = 0.034 \pm 0.008$ is the linear phase coefficient [4]. The line in Fig. 3-5 does not match the line plotted in Buratti et al. (2015) due to an error in the printed Fourier coefficients[1][4]. The printed coefficients correspond to a light curve in terms of flux, while the plot shows a light curve in terms of apparent magnitude. While the correct Fourier coefficients for the Buratti et al. (2015) fit have not yet been determined, the relationship between

[1]From email communication with B. J. Buratti and M. D. Hicks on January 14-20, 2016

flux and magnitude means that the shape of the curve is the opposite of what it should be, so that the fitted line should be concave up at lower longitudes and concave down at higher longitudes. With this correction applied, the general shape of the Buratti et al. (2015) fit would match the sinusoidal shape of the measurements taken at Wallace Observatory.

To confirm that the observed light curve is the correct general shape, its shape was compared to that of the model's synthetic light curve for Pluto in October of 2015, assuming no albedo change since the New Horizons flyby in July 2015. Additionally, both the model and the observational data were matched to the map of Pluto from New Horizons [8]. The results of these comparisons are shown in Fig. 3-6. In this figure, the output of the model is offset by $\Delta m = 1.52$ at all points in order to make the mean magnitude of the model match the observed mean magnitude. This correction was applied because the data were taken in the R filter, while the model does not apply any filters when calculating Pluto's magnitude. Therefore, the model produces brighter magnitudes than the observational data. While the observations are noisier than the synthetic light curve, they trace the same general shape. Additionally, the brightest part of the light curve corresponds to longitudes near Tombaugh Regio, while the darkest part corresponds to longitudes near Cthulhu Regio. These two regions are the brightest and darkest spots on Pluto, respectively, so this alignment confirms that the observations match the expected general shape of the light curve.

Additionally, to determine the amplitude of the observed light curve, a sinusoid of the form $m = a\sin(\lambda + b) + c$, where m is the apparent magnitude of Pluto and λ is the east longitude in radians. The results of this fit are shown in Fig. 3-7, along with the predicted light curve from the model. The best fit parameters were $a = 0.0622 \pm 0.0012$, $b = 0.603 \pm 0.012$, and $c = 14.6711 \pm 0.0006$, which correspond to a light curve amplitude of $\Delta m = 0.1245 \pm 0.0012$. This amplitude is slightly larger than Buratti et al. (2015)'s measurement of $\Delta m = 0.11 \pm 0.03$ in 2014[4]. However, it is smaller than the static-albedo model's prediction that the light curve amplitude would be $\Delta m = 0.1990$. The discrepancy between the observed amplitude and the model's predicted amplitude is most likely due to the fact that Pluto was very near

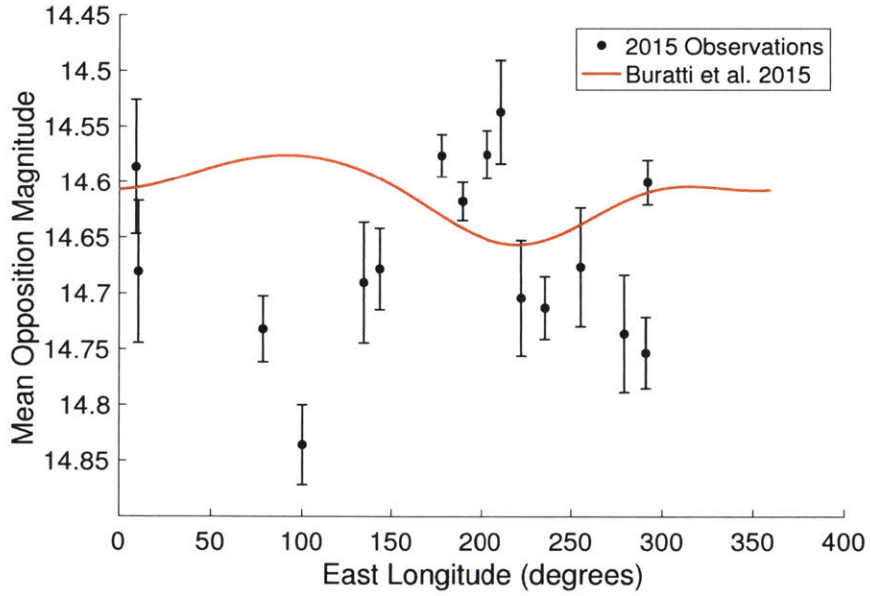

Figure 3-5: Pluto light curve created from our data, plotted with the fitted line from Fig. 1 Buratti et al. (2015) given by Eq. 3.3 [4]. The data are much noisier than the fitted line, which was taken as an indication that the amplitude of Pluto's light curve is currently too small to be well detected using the 16-inch telescope at Wallace Observatory. Note that the red line plotted here does not match the line in Fig. 1 of Buratti et al. (2015) because of an error in the printed Fourier coefficients. This error is being investigated by the paper authors but has yet to be resolved.

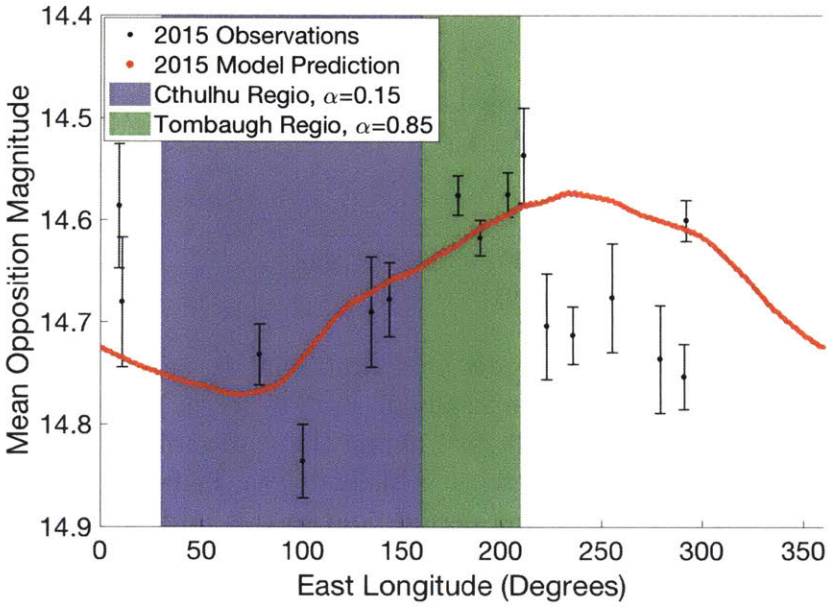

Figure 3-6: A comparison of observational data to the model's prediction. Observational data points are in black, while the red points indicate the synthetic light curve for October 2015, assuming that Pluto's albedo distribution has remained constant since the July 2015 New Horizons flyby. The blue and green regions indicate the general longitude ranges of Cthulhu Regio and Tombaugh Regio, which should be the darkest and brightest points of the light curve, respectively. While the observational data is more noisy than the model, the general shapes of the two data sets match, and both sets are darkest near Cthulhu Regio and brightest near Tombaugh Regio. This match indicates that the observational light curve is the right shape, despite the mismatch with the fitted line from Buratti et al. (2015)[4]. The discrepancy between these observations and the fitted line from Buratti et al. (2015) is due to an error in the published Fourier coefficients[4]. This error is being investigated by the paper authors but has yet to be resolved.

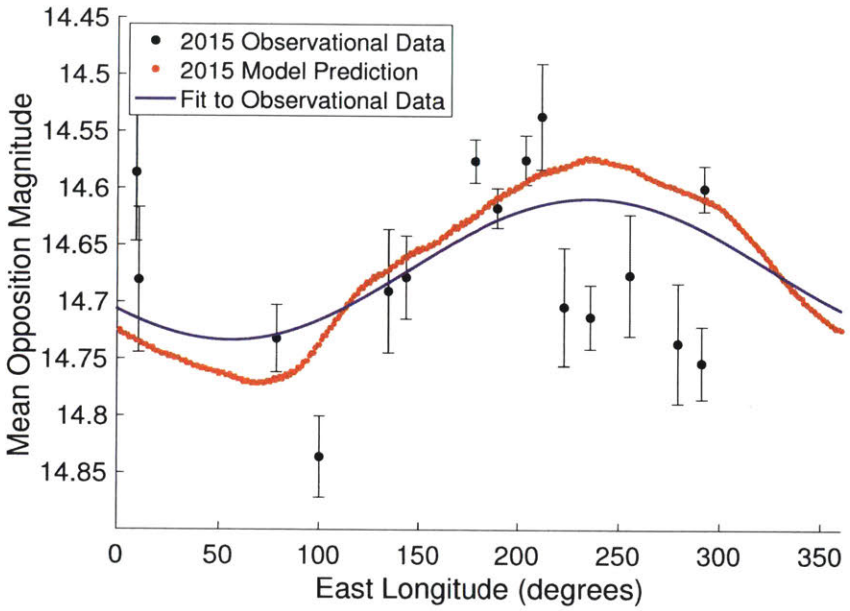

Figure 3-7: Observational data plotted with the best sinusoidal fit to the data (in blue) and the light curve predicted by the static-albedo model (in red). The model predicted a light curve amplitude of $\Delta m = 0.1990$, while the sinusoidal fit gave an amplitude of $\Delta m = 0.1245 \pm 0.0012$. This difference is likely due to the fact that Pluto was very near the horizon during the observing period, and so this added significant error to the measured magnitudes.

the horizon at the time of observation. At very low altitudes, the high airmass means that on-chip standard stars may have nonlinear refraction, so the on-chip standards provide less accurate measurements of Pluto's magnitude near the horizon.

Although the observational data did not exactly match the model because of the errors associated with observing Pluto at very low altitudes, the model can be used to predict when changes on Pluto will be observable on a variety of telescopes.

Chapter 4

Pluto's Future Observability

4.1 Wallace Observatory

While Pluto is observable on Wallace Observatory's 16-inch telescope, the purpose of observations of Pluto is to accurately measure changes in Pluto's mean magnitude and lightcurve amplitude over time in order to investigate volatile transport on Pluto's surface. The model developed in Section 2.1 can be applied to determine when changes in Pluto's mean magnitude would be detectable from Wallace Observatory and using a range of other telescope sizes.

Fig. 4-1 graphs the change in Pluto's mean magnitude over 1-year, 2-year, and 3-year timescales for the static albedo model. Although this plot displays how Pluto's magnitude changes on different timescales due purely to geometric effects, its albedo distribution can also affect its observed magnitude. As described in Section 2.2, the most likely change in Pluto's albedo that would be visible from Earth is a darkening of the bright North Pole region [6]. The effects of this albedo change were investigated by converting part or all of the $\alpha = 0.7$ North Pole area to a material closer to the dark equatorial regions, with $\alpha = 0.4$. Fig. 4-2 shows the results of a model in which the entire pole is sublimated to a material with $\alpha = 0.4$ over a timescale of one, two, or three years.

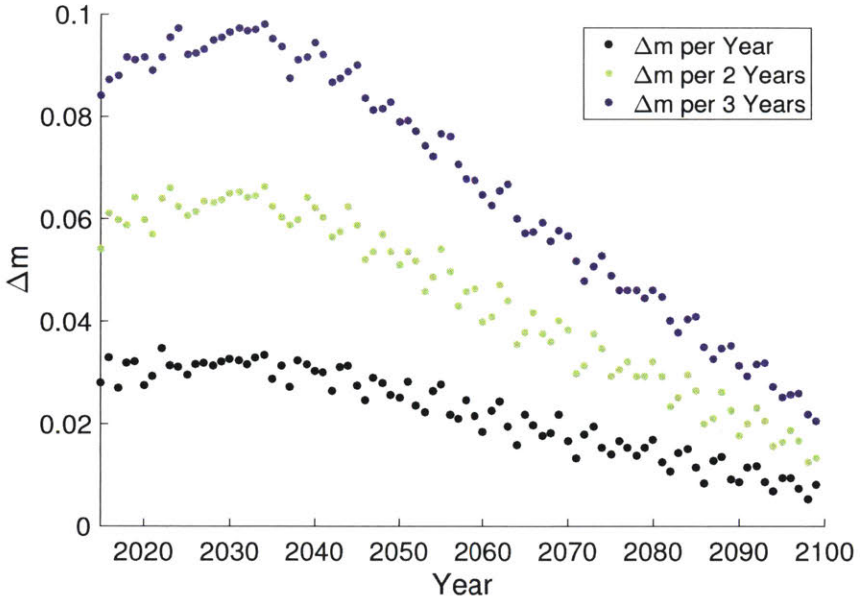

Figure 4-1: Change in Pluto's mean magnitude, assuming a static albedo distribution. Black, green, and blue points indicate the magnitude change over timescales of one, two, and three years, respectively. If Pluto's albedo distribution were constant over time, than a yearly change in magnitude of about $\Delta m = 0.02$ would be observed.

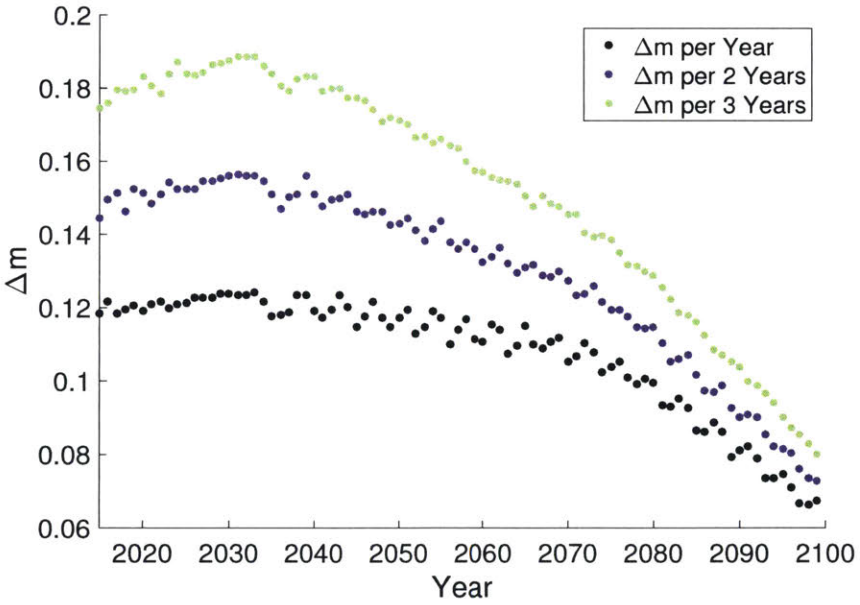

Figure 4-2: Change in Pluto's mean magnitude, assuming the entire North Pole region above 60°latitude is sublimated to reveal a surface with an albedo of $\alpha = 0.4$. Black, green, and blue points indicate the magnitude change over timescales of one, two, and three years, respectively. If Pluto's entire pole sublimated over the course of a year, a change in magnitude of about $\Delta m = 0.1$ would be observed.

4.2 Other Telescopes

While Pluto is observable using the 16-inch telescope at Wallace Observatory, larger telescopes can detect smaller magnitude changes and will therefore be better able to observe changes in Pluto's light curve. Given a length of observation time, the smallest change in magnitude detectable by a given telescope depends on the telescope's diameter. Therefore, to investigate what magnitude changes were observable on a variety of telescope sizes, a constant observation time of 10 minutes was used to calculate the signal from Pluto and the theoretical signal-to-noise ratio. This time was chosen because, to properly obtain a light curve of Pluto's 6.4-day rotational period, observations must be taken on seven different nights. To observe Pluto on seven separate nights on a large telescope such as the 6.5-meter Magellan telescopes, a small amount of observing time would need to be obtained on each night. Therefore, approximately one hour of observing time could be expected each night. However, standard stars must also be observed during this one-hour time window. To observe Pluto, which is at a magnitude of approximately $m = 14.6$, as well as four Landolt standard stars, which are at magnitudes between $m = 11$ and $m = 14$, approximately 45 minutes of the observing hour may be spent on the standard stars, while 15 minutes would be spent on observing Pluto. 15 minutes of time observing Pluto corresponds to about 10 minutes of integration time, so this length of time was used to calculate the smallest change in Pluto's magnitude visible on each telescope.

In addition to the length of observing time and telescope size, the altitude at which Pluto is observed will also play a role in determining what the smallest observable change in magnitude is, because at a lower altitude Pluto will be observed through a larger airmass and will appear fainter. For the 6.5-m telescope limit, it was assumed that Pluto would be observed at an altitude of $Alt = 45°$, because the Magellan telescopes are in the Southern hemisphere and therefore can observe Pluto at these higher altitudes. However, for all other telescope limits, it was assumed that Pluto would be observed from the Northern hemisphere, where it rises to a maximum altitude of $Alt = 25°$. Therefore, an altitude of 25° was used to calculate the extinction

Table 4.1: The theoretical three-sigma accuracy limit for a variety of different telescope sizes. The accuracy limit depends on the telescope diameter, because a larger telescope will be able to detect smaller amplitude changes.

Diameter (m)	Observability Limit
6.5	0.0001
4	0.0002
2	0.0003
1	0.0008
0.6096	0.0011
0.4064	0.0017

for all telescopes except the 6.5-m telescope. For data taken in the R filter, a typical value for the extinction coefficient is $k_R = 0.11$, so this extinction coefficient was assumed to apply to all of the telescope sizes[13]. The magnitude limits calculated from combining these observational parameters are summarized in Table 4.1.

Fig. 4-3 plots the change in Pluto's magnitude over a one-year period for a set of different Pluto models. The static-albedo model in one in which Pluto's North Pole region is completely covered in material with an albedo of $\alpha = 0.7$ at all times. The other models graphed all represent albedo maps in which some percentage of the $\alpha = 0.7$ polar region was converted to a material with $\alpha = 0.4$. As Fig. 4-3 shows, the change in Pluto's mean magnitude over one year is well above the observability limits for all of the telescopes considered in Table 4.1 even when only geometry changes, and not surface changes, are considered, assuming that Pluto is observed at a high enough altitude to obtain accurate photometry. This graph can also be used to interpret future observations of Pluto because it shows what magnitude change is expected for a variety of surface albedo distributions on Pluto.

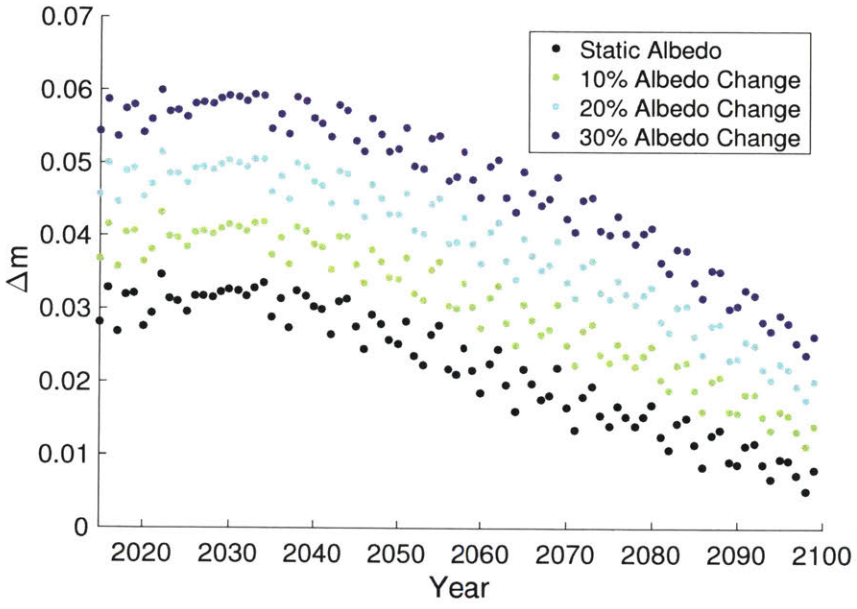

Figure 4-3: Change in magnitude per year for a variety of Pluto models. The black points represent a static-albedo model in which there are no changes in Pluto's albedo distribution over time. The green, cyan, and blue points represent models in which, over the course of one year, 10%, 20%, and 30% of Pluto's North Pole region above 60° latitude has been changed from a material with albedo $\alpha = 0.7$ to one with albedo $\alpha = 0.4$, respectively. The scatter within each of the curves is believed to be due to the resolution of the albedo map. These data can be used to interpret future observations and determine what surface change would produced the observed magnitude change.

Chapter 5

Conclusions

As indicated by the magnitude changes predicted by the model, yearly observations of Pluto using the Magellan telescopes can provide useful information about changes to Pluto's surface. Observations of Pluto on smaller telescopes would also be sensitive enough to see changes in Pluto's light curve if they are conducted at high enough altitudes to result in accurate photometry. The model can be used to plan future observations by providing predictions of Pluto's magnitude and light curve amplitude. Additionally, if later observations display different magnitude changes than those predicted by the static albedo model, this could be an indication of volatile transport causing surface albedo changes. Comparison to the model can give an estimate of the amount of change in the surface albedo distribution necessary to produce the observed light curve change. While New Horizons only provided a picture of Pluto's surface at one point in time, continued observations can detect how its surface evolves as its insolation changes. Continuing to observe Pluto on larger ground-based telescopes in the future, and using this model to interpret those observations, will allow further investigation into the processes of volatile transport on its surface and how those processes are driven by variations in insolation.

Appendix A

APASS Standard Stars

The APASS standard stars used to calculate the magnitude of Pluto, as described in Section 3.2.1, are listed in Table A.1. The table lists the positions of each star and their magnitudes in all filters measured by the APASS survey. Figures A-1 throughA-16 display the relative positions of Pluto and the comparison stars on each night of observations.

Table A.1: Table of magnitudes and positions of APASS standard stars used to compute the magnitude of Pluto, sorted by the night on which they appeared on-chip with Pluto. All RA and Declination values are in degrees.

Date Observed	RA	Dec	Johnson V	Johnson B	Sloan g'	Sloan r'	Sloan i'
	283.578132	-21.03255	13.586	14.631	14.105	13.208	12.884
	283.584312	-21.031208	14.491	15.955	15.207	13.978	13.547
	283.596652	-21.022073	13.532	14.204	13.841	13.314	13.112
	283.618878	-20.945263	14.3	15.599	14.926	13.802	13.423
	283.625185	-21.013909	14.439	15.658	14.997	13.999	13.646
	283.644891	-21.046512	14.272	15.409	14.812	13.885	13.566
	283.647273	-20.994937	13.713	15.014	14.339	13.242	12.843
2015/09/19	283.653179	-21.001313	14.099	14.819	14.434	13.844	13.731

	283.661706	-21.032563	13.654	14.993	14.305	13.198	12.853
	283.668098	-21.035477	14.414	15.65	14.97	13.994	13.628
	283.67625	-21.101226	13.91	15.531	14.589	13.393	12.911
	283.68404	-20.996801	13.266	13.871	13.515	13.062	12.95
	283.760168	-20.956921	13.408	14.107	13.738	13.194	13.043
	283.760404	-20.991391	13.762	14.79	14.201	13.39	13.066
	283.760413	-21.054175	13.966	15.155	14.55	13.504	13.142
	283.591084	-20.964749	13.509	15.371	14.419	12.813	11.995
	283.592762	-20.987926	13.481	14.985	14.243	12.932	12.361
	283.596652	-21.022073	13.532	14.204	13.841	13.314	13.112
	283.603602	-20.984752	14.619	15.882	15.202	14.176	13.771
	283.608865	-21.067607	14.545	15.362	14.928	14.28	14.108
	283.616272	-21.09589	14.3	15.621	14.941	13.832	13.48
	283.618878	-20.945263	14.3	15.599	14.926	13.802	13.423
	283.619111	-21.065304	14.571	15.713	15.128	14.164	13.858
	283.623728	-21.089218	14.507	15.331	14.905	14.247	14.084
2015/09/20	283.625185	-21.013909	14.439	15.658	14.997	13.999	13.646
	283.636331	-21.094237	14.784	16.177	15.437	14.335	13.963
	283.636569	-20.950323	14.384	15.563	14.971	13.997	13.599
	283.638312	-20.932799	14.041	15.49	14.746	13.493	13
	283.644891	-21.046512	14.272	15.409	14.812	13.885	13.566
	283.647273	-20.994937	13.713	15.014	14.339	13.242	12.843
	283.653179	-21.001313	14.099	14.819	14.434	13.844	13.731
	283.661706	-21.032563	13.654	14.993	14.305	13.198	12.853
	283.67625	-21.101226	13.91	15.531	14.589	13.393	12.911
	283.68404	-20.996801	13.266	13.871	13.515	13.062	12.95
	283.574472	-21.048335	14.173	15.717	14.948	13.59	13.032
	283.625185	-21.013909	14.439	15.658	14.997	13.999	13.646
	283.644891	-21.046512	14.272	15.409	14.812	13.885	13.566
2015/09/24	283.67625	-21.101226	13.91	15.531	14.589	13.393	12.911

	283.68404	-20.996801	13.266	13.871	13.515	13.062	12.95
	283.685083	-21.073765	14.268	15.532	14.833	13.792	13.512
2015/09/26	283.596652	-21.022073	13.532	14.204	13.841	13.314	13.112
	283.634188	-21.11785	14.202	15.109	14.59	13.901	13.738
	283.653179	-21.001313	14.099	14.819	14.434	13.844	13.731
	283.661706	-21.032563	13.654	14.993	14.305	13.198	12.853
	283.668098	-21.035477	14.414	15.65	14.97	13.994	13.628
	283.668806	-21.07982	14.222	15.463	14.942	13.836	13.58
	283.67625	-21.101226	13.91	15.531	14.589	13.393	12.911
	283.685083	-21.073765	14.268	15.532	14.833	13.792	13.512
	283.745392	-21.095179	14.237	15.224	14.699	13.948	13.69
	283.760404	-20.991391	13.762	14.79	14.201	13.39	13.066
	283.760413	-21.054175	13.966	15.155	14.55	13.504	13.142
	283.764114	-21.081922	13.504	14.614	14.02	13.139	12.818
2015/09/27	283.574472	-21.048335	14.173	15.717	14.948	13.59	13.032
	283.584312	-21.031208	14.491	15.955	15.207	13.978	13.547
	283.596652	-21.022073	13.532	14.204	13.841	13.314	13.112
	283.625185	-21.013909	14.439	15.658	14.997	13.999	13.646
	283.634188	-21.11785	14.202	15.109	14.59	13.901	13.738
	283.644891	-21.046512	14.272	15.409	14.812	13.885	13.566
	283.647273	-20.994937	13.713	15.014	14.339	13.242	12.843
	283.661706	-21.032563	13.654	14.993	14.305	13.198	12.853
	283.668098	-21.035477	14.414	15.65	14.97	13.994	13.628
	283.67625	-21.101226	13.91	15.531	14.589	13.393	12.911
	283.68404	-20.996801	13.266	13.871	13.515	13.062	12.95
2015/10/10	283.644891	-21.046512	14.272	15.409	14.812	13.885	13.566
	283.67625	-21.101226	13.91	15.531	14.589	13.393	12.911
	283.68404	-20.996801	13.266	13.871	13.515	13.062	12.95
	283.720642	-21.138429	14.397	16.122	15.232	13.73	13.027
	283.742261	-21.115095	13.647	15.165	14.324	13.162	12.648

	283.745392	-21.095179	14.237	15.224	14.699	13.948	13.69
	283.75184	-21.141986	14.139	15.366	14.747	13.714	13.392
	283.760404	-20.991391	13.762	14.79	14.201	13.39	13.066
	283.760413	-21.054175	13.966	15.155	14.55	13.504	13.142
	283.794427	-21.12107	13.737	14.421	14.05	13.546	13.421
	283.805009	-21.038558	13.658	14.694	14.161	13.294	12.946
2015/10/11	283.644891	-21.046512	14.272	15.409	14.812	13.885	13.566
	283.661706	-21.032563	13.654	14.993	14.305	13.198	12.853
	283.668098	-21.035477	14.414	15.65	14.97	13.994	13.628
	283.668806	-21.07982	14.222	15.463	14.942	13.836	13.58
	283.67625	-21.101226	13.91	15.531	14.589	13.393	12.911
	283.68404	-20.996801	13.266	13.871	13.515	13.062	12.95
	283.720642	-21.138429	14.397	16.122	15.232	13.73	13.027
	283.742261	-21.115095	13.647	15.165	14.324	13.162	12.648
	283.745392	-21.095179	14.237	15.224	14.699	13.948	13.69
	283.75184	-21.141986	14.139	15.366	14.747	13.714	13.392
	283.760404	-20.991391	13.762	14.79	14.201	13.39	13.066
	283.760413	-21.054175	13.966	15.155	14.55	13.504	13.142
	283.764114	-21.081922	13.504	14.614	14.02	13.139	12.818
	283.777657	-21.110633	14.178	15.704	14.894	13.692	13.216
	283.778629	-21.117179	13.735	14.993	14.305	13.289	12.847
	283.794427	-21.12107	13.737	14.421	14.05	13.546	13.421
	283.805009	-21.038558	13.658	14.694	14.161	13.294	12.946
	283.82598	-21.053812	13.629	14.73	14.114	13.184	12.727
	283.83589	-21.089345	14.218	15.375	14.748	13.787	13.378
	283.844113	-21.063478	14.375	15.698	14.986	13.879	13.413
2015/10/12	283.668098	-21.035477	14.414	15.65	14.97	13.994	13.628
	283.67625	-21.101226	13.91	15.531	14.589	13.393	12.911
	283.720642	-21.138429	14.397	16.122	15.232	13.73	13.027
	283.745392	-21.095179	14.237	15.224	14.699	13.948	13.69

	283.75184	-21.141986	14.139	15.366	14.747	13.714	13.392
	283.760404	-20.991391	13.762	14.79	14.201	13.39	13.066
	283.760413	-21.054175	13.966	15.155	14.55	13.504	13.142
	283.794427	-21.12107	13.737	14.421	14.05	13.546	13.421
	283.801749	-21.15722	13.849	15.213	14.524	13.439	13.002
	283.805009	-21.038558	13.658	14.694	14.161	13.294	12.946
2015/10/16	283.742261	-21.115095	13.647	15.165	14.324	13.162	12.648
	283.745392	-21.095179	14.237	15.224	14.699	13.948	13.69
	283.75184	-21.141986	14.139	15.366	14.747	13.714	13.392
	283.760404	-20.991391	13.762	14.79	14.201	13.39	13.066
	283.760413	-21.054175	13.966	15.155	14.55	13.504	13.142
	283.794427	-21.12107	13.737	14.421	14.05	13.546	13.421
	283.801749	-21.15722	13.849	15.213	14.524	13.439	13.002
	283.805009	-21.038558	13.658	14.694	14.161	13.294	12.946
	283.82598	-21.053812	13.629	14.73	14.114	13.184	12.727
	283.844113	-21.063478	14.375	15.698	14.986	13.879	13.413
	283.845002	-21.158893	13.923	14.511	14.165	13.755	13.628
	283.854406	-21.118489	14.352	15.686	14.974	13.819	12.243
	283.860996	-21.086782	14.012	15.612	14.758	13.405	12.64
	283.863797	-21.013452	13.896	15.556	14.72	13.307	12.483
2015/10/18	283.742261	-21.115095	13.647	15.165	14.324	13.162	12.648
	283.745392	-21.095179	14.237	15.224	14.699	13.948	13.69
	283.760413	-21.054175	13.966	15.155	14.55	13.504	13.142
	283.764114	-21.081922	13.504	14.614	14.02	13.139	12.818
	283.777657	-21.110633	14.178	15.704	14.894	13.692	13.216
	283.778629	-21.117179	13.735	14.993	14.305	13.289	12.847
	283.794427	-21.12107	13.737	14.421	14.05	13.546	13.421
	283.801749	-21.15722	13.849	15.213	14.524	13.439	13.002
	283.805009	-21.038558	13.658	14.694	14.161	13.294	12.946
	283.80532	-20.99914	14.08	15.651	14.82	13.464	12.768

	283.82598	-21.053812	13.629	14.73	14.114	13.184	12.727
	283.83589	-21.089345	14.218	15.375	14.748	13.787	13.378
	283.844113	-21.063478	14.375	15.698	14.986	13.879	13.413
	283.845002	-21.158893	13.923	14.511	14.165	13.755	13.628
	283.860996	-21.086782	14.012	15.612	14.758	13.405	12.64
	283.863797	-21.013452	13.896	15.556	14.72	13.307	12.483
	283.875304	-21.109514	13.618	14.715	14.134	13.276	12.958
	283.82598	-21.053812	13.629	14.73	14.114	13.184	12.727
	283.83589	-21.089345	14.218	15.375	14.748	13.787	13.378
	283.844113	-21.063478	14.375	15.698	14.986	13.879	13.413
	283.844564	-21.091719	13.955	14.951	14.469	13.606	13.33
	283.845002	-21.158893	13.923	14.511	14.165	13.755	13.628
	283.854406	-21.118489	14.352	15.686	14.974	13.819	12.243
	283.860996	-21.086782	14.012	15.612	14.758	13.405	12.64
2015/10/23	283.863797	-21.013452	13.896	15.556	14.72	13.307	12.483
	283.875304	-21.109514	13.618	14.715	14.134	13.276	12.958
	283.885178	-21.125691	14.035	15.319	14.669	13.627	13.162
	283.905892	-21.169884	13.782	14.556	14.129	13.55	13.342
	283.918612	-21.026399	13.738	14.874	14.313	13.299	12.876
	283.934634	-21.174954	13.939	15.102	14.571	13.528	13.185
	283.973299	-21.126782	13.851	14.697	14.263	13.649	13.435
	284.009141	-21.083137	14.222	15.377	14.773	13.878	13.459
	283.860996	-21.086782	14.012	15.612	14.758	13.405	12.64
	283.875304	-21.109514	13.618	14.715	14.134	13.276	12.958
	283.906385	-21.073203	13.863	15.059	14.401	13.441	13.053
2015/10/26	283.918612	-21.026399	13.738	14.874	14.313	13.299	12.876
	283.934634	-21.174954	13.939	15.102	14.571	13.528	13.185
	284.006455	-21.010979	13.321	14.08	13.668	13.094	12.866
	284.009141	-21.083137	14.222	15.377	14.773	13.878	13.459
	283.973299	-21.126782	13.851	14.697	14.263	13.649	13.435

	283.984247	-21.13276	13.617	14.875	14.219	13.209	12.795
	284.006455	-21.010979	13.321	14.08	13.668	13.094	12.866
	284.007055	-21.103021	14.151	15.353	14.727	13.763	13.354
	284.009141	-21.083137	14.222	15.377	14.773	13.878	13.459
	284.012753	-21.050215	13.433	13.991	13.686	13.271	13.119
	284.046832	-20.997903	14.229	15.417	14.846	13.754	13.402
	284.054639	-21.055339	13.551	15.089	14.299	13.075	12.483
	284.056008	-21.061337	14.036	15.262	14.631	13.655	13.257
	284.06484	-21.018404	13.331	14.414	13.901	13.042	12.665
	284.072513	-21.062387	14.19	15.585	14.869	13.623	13.084
	284.073768	-21.091856	13.971	15.127	14.549	13.633	13.299
	284.087224	-21.043025	14.049	15.384	14.656	13.523	13.01
	284.092154	-21.018669	13.734	15.489	14.659	13.12	12.205
	284.097002	-21.162239	14.067	15.255	14.652	13.703	13.259
	284.124992	-21.101124	13.531	14.137	13.832	13.346	13.101
	284.007055	-21.083137	14.222	15.377	14.773	13.878	13.459
	284.065806	-21.062387	14.19	15.585	14.869	13.623	13.084
	284.097002	-21.101124	13.531	14.137	13.832	13.346	13.101
2015/11/03	284.124992	-21.013602	14.145	15.159	14.688	13.746	13.41
	284.157626	-21.120126	13.991	14.705	14.323	13.777	13.545
	284.157919	-21.021185	13.643	14.776	14.187	13.299	12.92
	284.175944	-21.060281	13.266	14.023	13.632	13.03	12.74
	284.061076	-21.018404	13.331	14.414	13.901	13.042	12.665
	284.065806	-21.062387	14.19	15.585	14.869	13.623	13.084
	284.072513	-21.091856	13.971	15.127	14.549	13.633	13.299
2015/11/04	284.087224	-21.018669	13.734	15.489	14.659	13.12	12.205
	284.097002	-21.101124	13.531	14.137	13.832	13.346	13.101
	284.157626	-21.120126	13.991	14.705	14.323	13.777	13.545
	284.157679	-21.128843	14.401	16.218	15.211	13.744	12.196

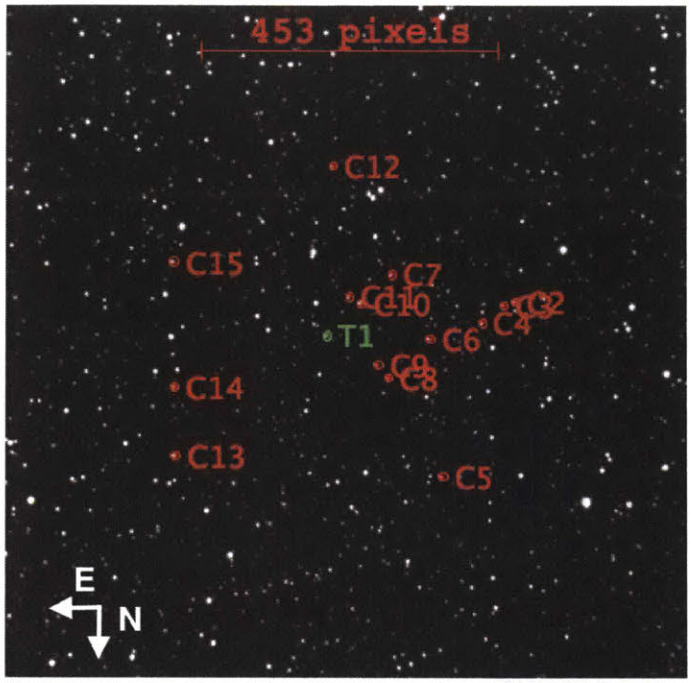

Figure A-1: Raw image of Pluto taken on September 19, 2015 at Wallace Observatory ($\phi = 4236.6'$, $\lambda = -7129.1'$), using the 14-inch telescope. Pluto is marked in green, while the positions of each APASS standard star used in analysis are marked in red.

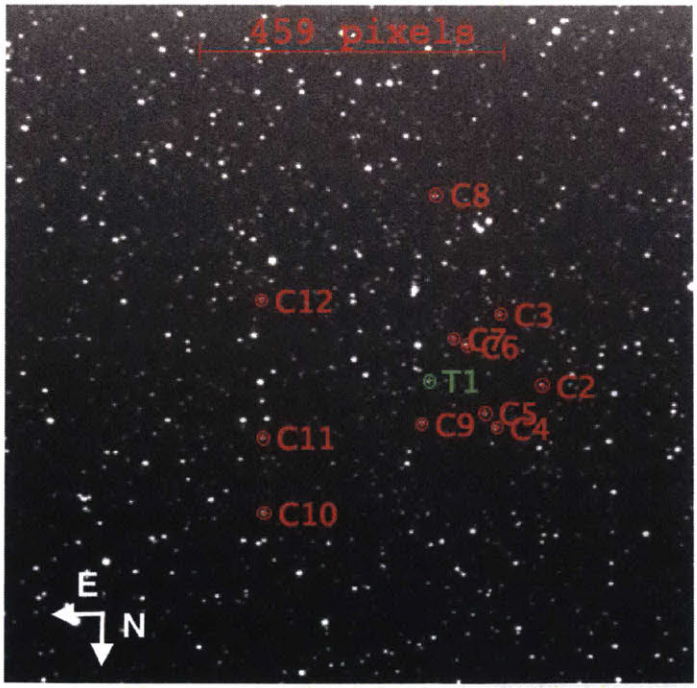

Figure A-2: Raw image of Pluto taken on September 19, 2015 at Wallace Observatory ($\phi = 4236.6'$, $\lambda = -7129.1'$), using the 16-inch telescope. Pluto is marked in green, while the positions of each APASS standard star used in analysis are marked in red.

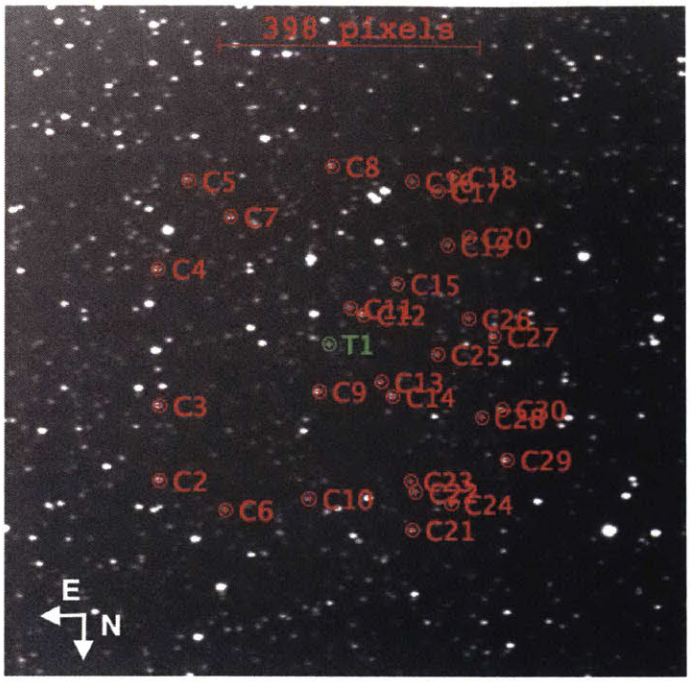

Figure A-3: Same as Fig. A-2, but for September 20, 2015.

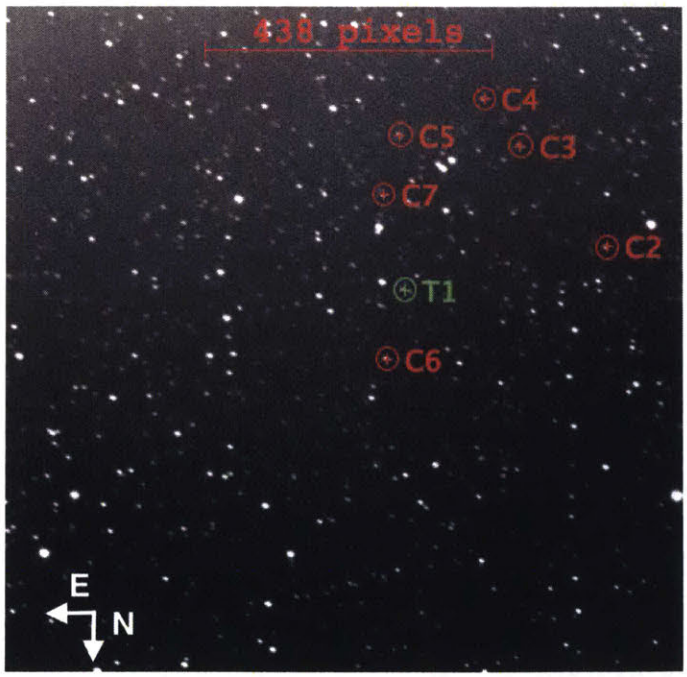

Figure A-4: Same as Fig. A-2, but for September 24, 2015.

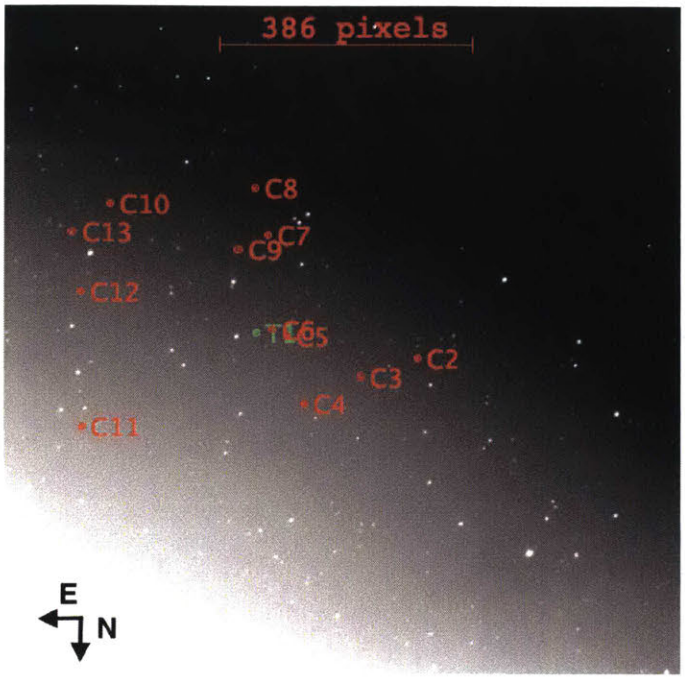

Figure A-5: Same as Fig. A-2, but for September 26, 2015.

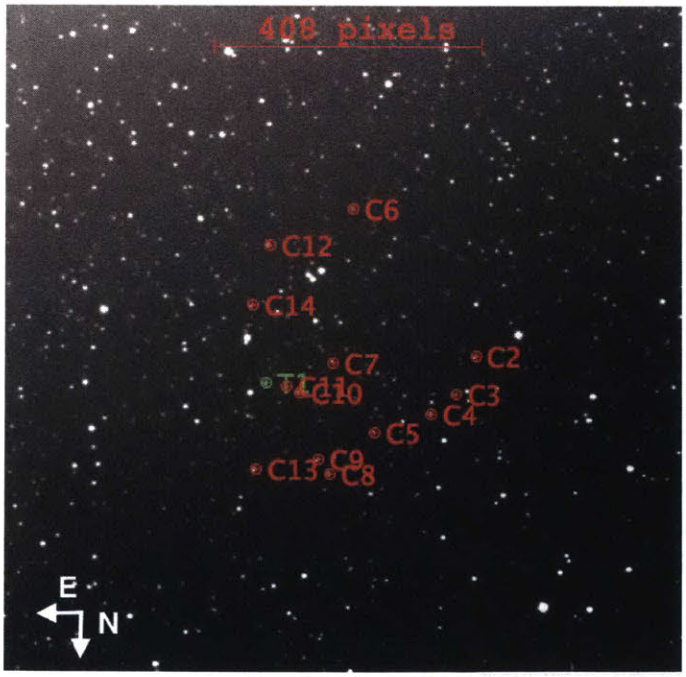

Figure A-6: Same as Fig. A-2, but for September 27, 2015.

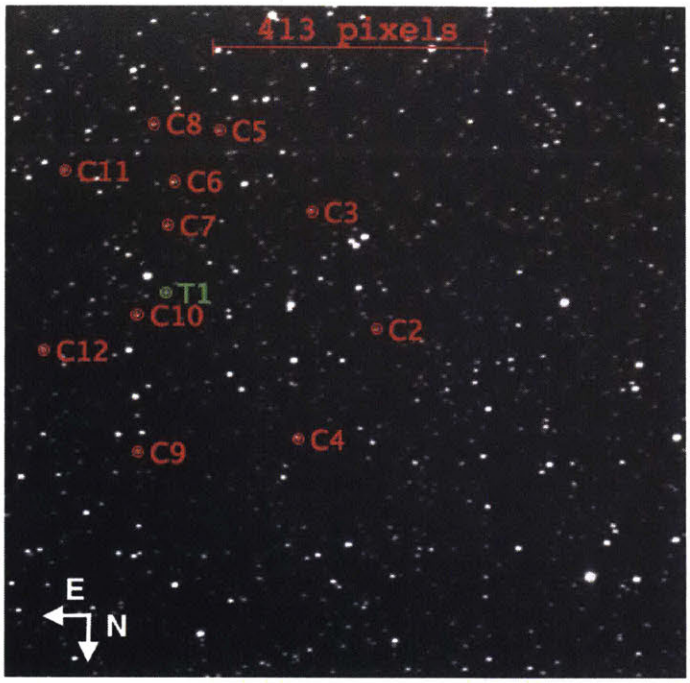

Figure A-7: Same as Fig. A-2, but for October 10, 2015.

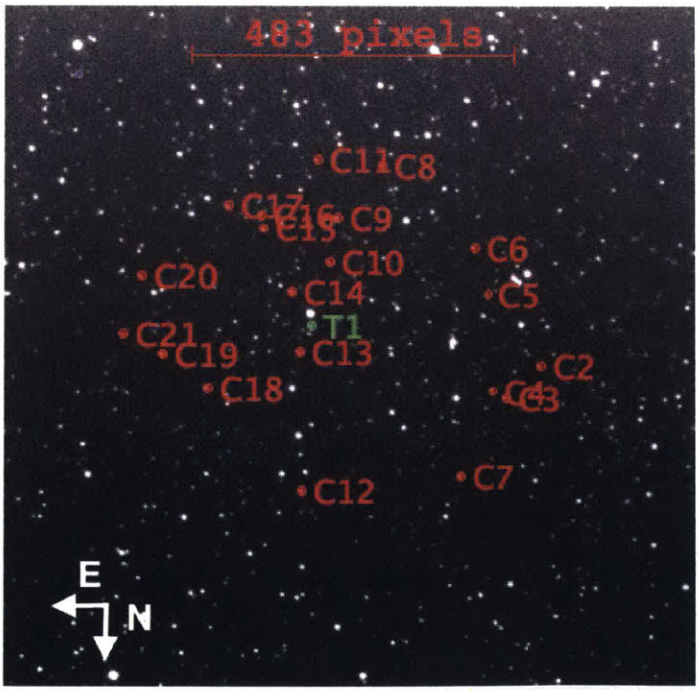

Figure A-8: Same as Fig. A-2, but for October 11, 2015.

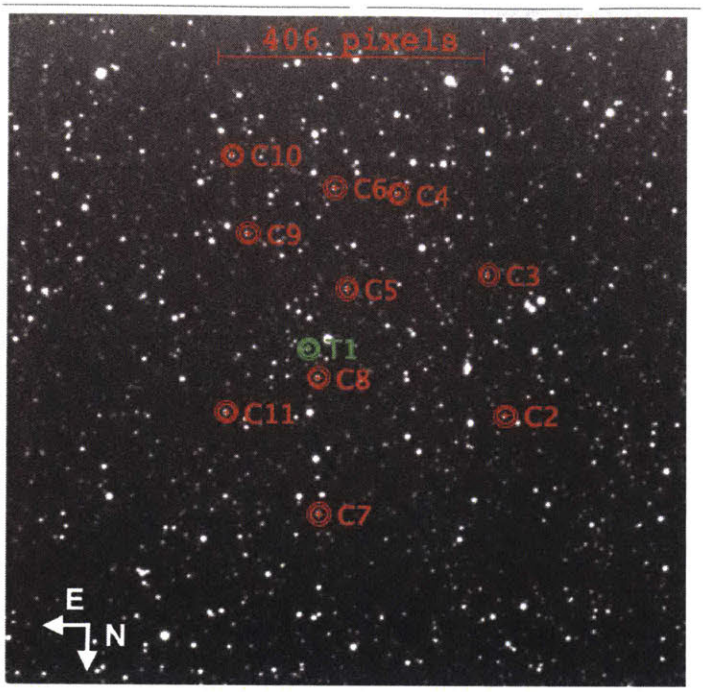

Figure A-9: Same as Fig. A-2, but for October 12, 2015.

Figure A-10: Same as Fig. A-2, but for October 16, 2015.

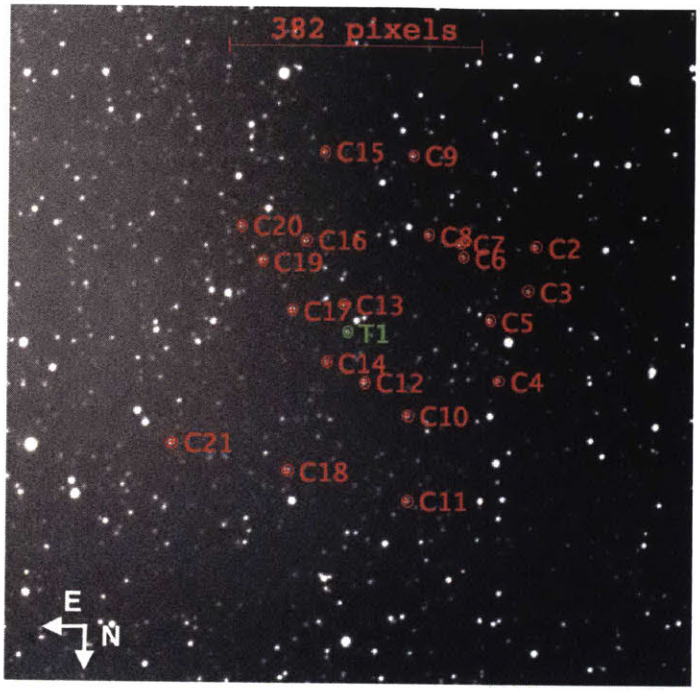

Figure A-11: Same as Fig. A-2, but for October 18, 2015.

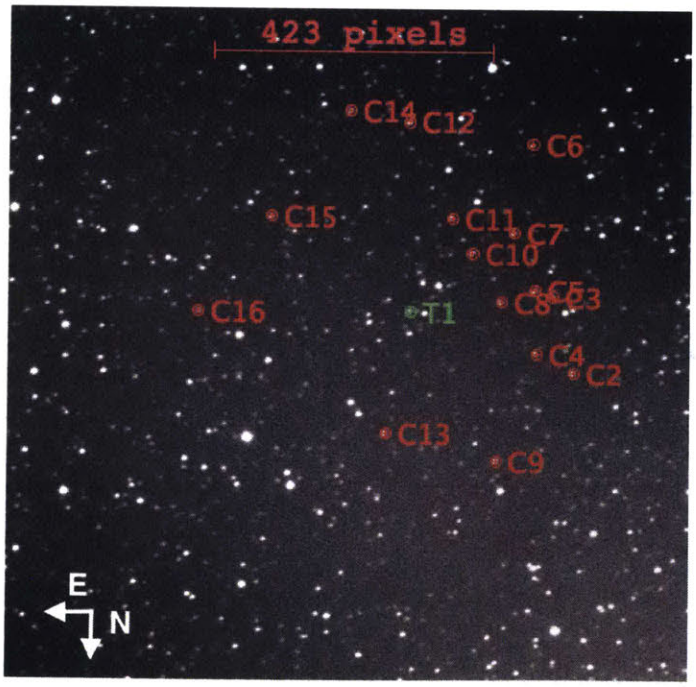

Figure A-12: Same as Fig. A-2, but for October 23, 2015.

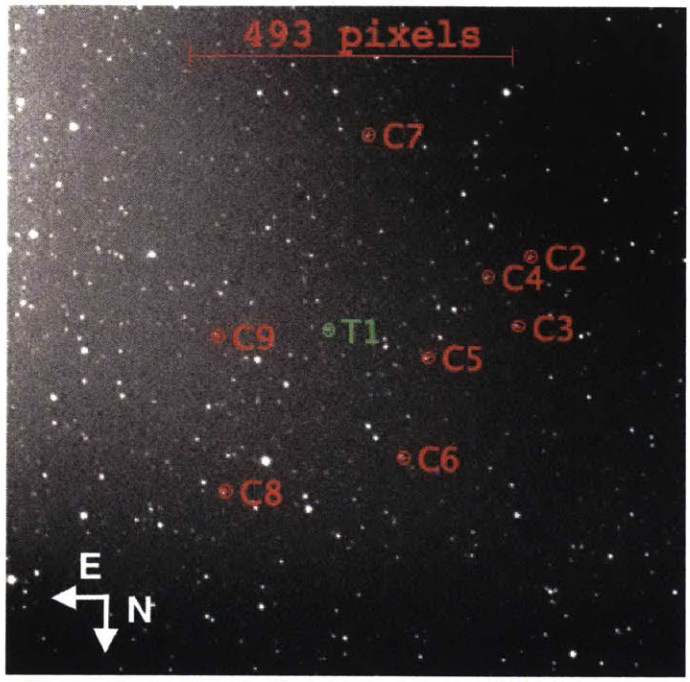

Figure A-13: Same as Fig. A-2, but for October 26, 2015.

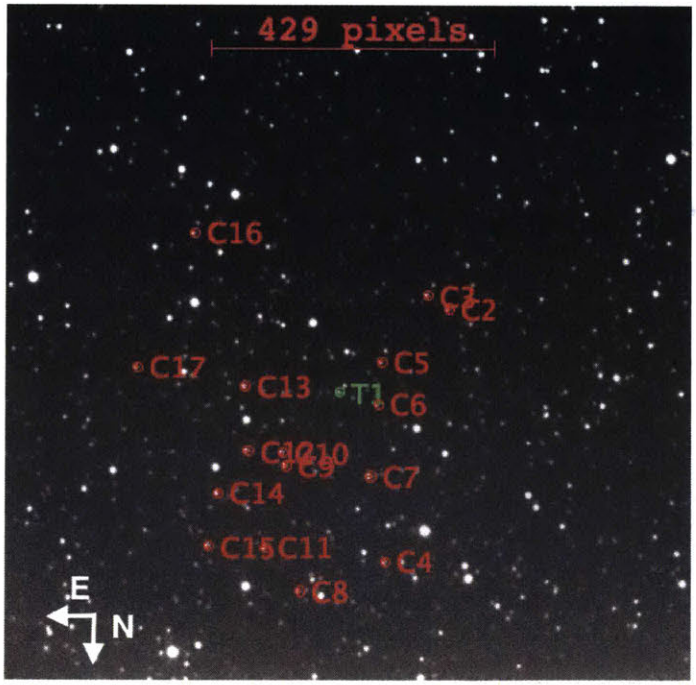

Figure A-14: Same as Fig. A-2, but for October 30, 2015.

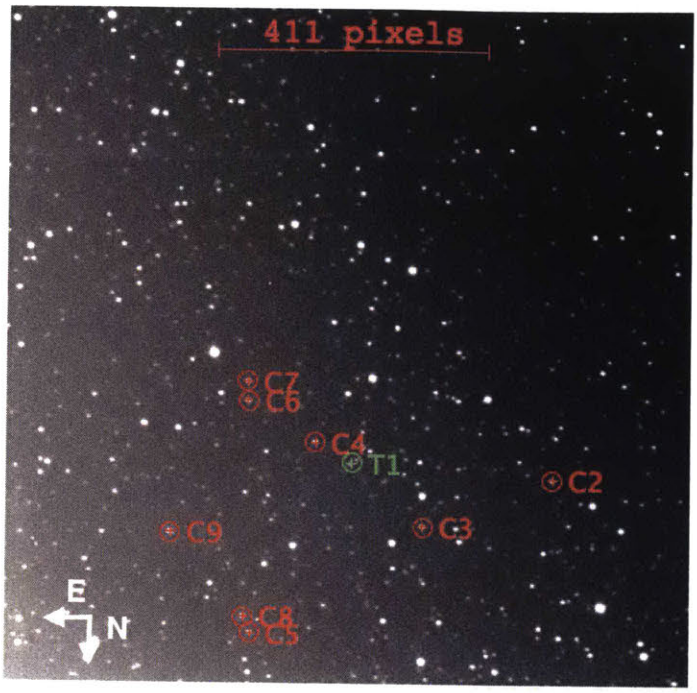

Figure A-15: Same as Fig. A-2, but for November 3, 2015.

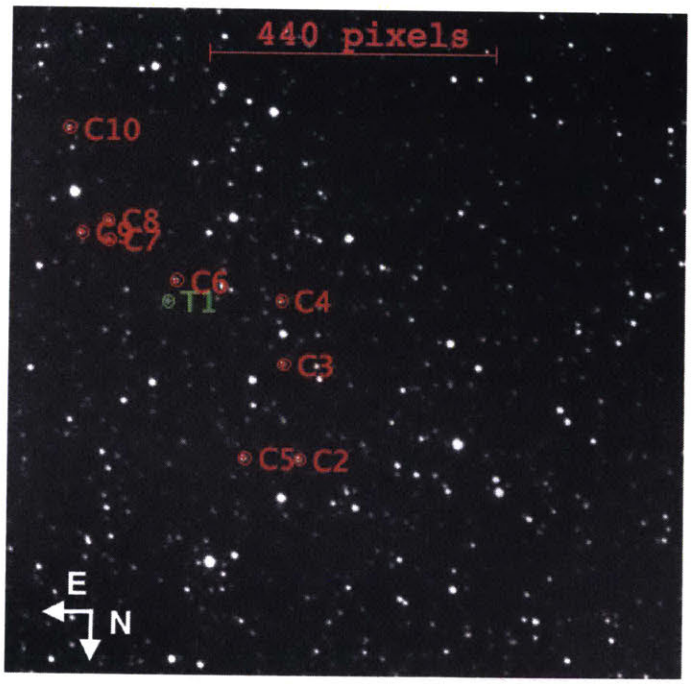

Figure A-16: Same as Fig. A-2, but for November 4, 2015.

Bibliography

[1] Michael E. Brown. Pluto and charon: Formation, seasons, composition. *Annual Review of Earth and Planetary Sciences*, 30:307–45, 2002.

[2] Marc W. Buie, William M. Grundy, Eliot F. Young, Leslie A. Young, and S. Alan Stern. Pluto and charon with the hubble space telescope. i. monitoring global change and improved surface properties from light curves. *The Astronomical Journal*, 139(3):1117–27, March 2010.

[3] Marc W. Buie, David J. Tholen, and Lawrence H. Wasserman. Separate lightcurves of pluto and charon. *Icarus*, 125(2):233–44, February 1997.

[4] B. J. Buratti, M. D. Hicks, P. A. Dalba, Devin Chu, Ariel O'Neill, J. K. Hillier, J. Masiero, Sophianna Banholzer, and H. Rhoades. Photometry of pluto 2008-2014: Evidence of ongoing seasonal volatile transport and activity. *The Astrophysical Journal Letters*, 804(1), April 2015.

[5] B. J. Buratti, J. K. Hillier, A. Heinze, M. D. Hicks, K. A. Tryka, J. A. Mosher, J. Ward, M. Garske, J. Young, and J. Atienza-Rosel. Photometry of pluto in the last decade and before: Evidence for volatile transport? *Icarus*, 162(1):171–82, 2003.

[6] Alissa M. Earle and Richard P. Binzel. Pluto's insolation history: Latitudinal variations and effects on atmospheric pressure. *Icarus*, 250:405–12, 2015.

[7] JD Giorgini and JPL Solar System Dynamics Group. Nasa/jpl horizons on-line ephemeris system. Web, March 2016.

[8] W.M. Grundy, R.P. Binzel, B.J. Buratti, J.C. Cook, D.P. Cruikshank, et al. Surface compositions across pluto and charon. *Science*, 351(6279):1283–91, March 2016.

[9] Candice J. Hansen and David A. Paige. Seasonal nitrogen cycles on pluto. *Icarus*, 120:247–65, 1996.

[10] K. Jordi, E. K. Grebel, and K. Ammon. Empirical color transformations between sdss photometry and other photometric systems. *Astronomy and Astrophysics*, 460(1):339–47, August 2006.

[11] S.A. Stern, F. Bagenal, K. Ennico, G.R. Gladstone, W.M. Grundy, et al. The pluto system: Initial results from its exploration by new horizons. *Science*, 350(6258):1–8, 2015.

[12] S.A. Stern, M.W.Buie, and L.M.Trafton. Hst high-resolution images and maps of pluto. *The Astronomical Journal*, 113(2):827–43, February 1997.

[13] H. Sung and M. S. Bessell. Standard stars: Ccd photometry, transformations and comparisons. *Publications of the Astronomical Society of Australia*, 17(3):244–54, August 2000.

[14] L. A. Young. Pluto's seasons: New predictions for new horizons. *The Astrophysical Journal Letters*, 766(2), March 2013.